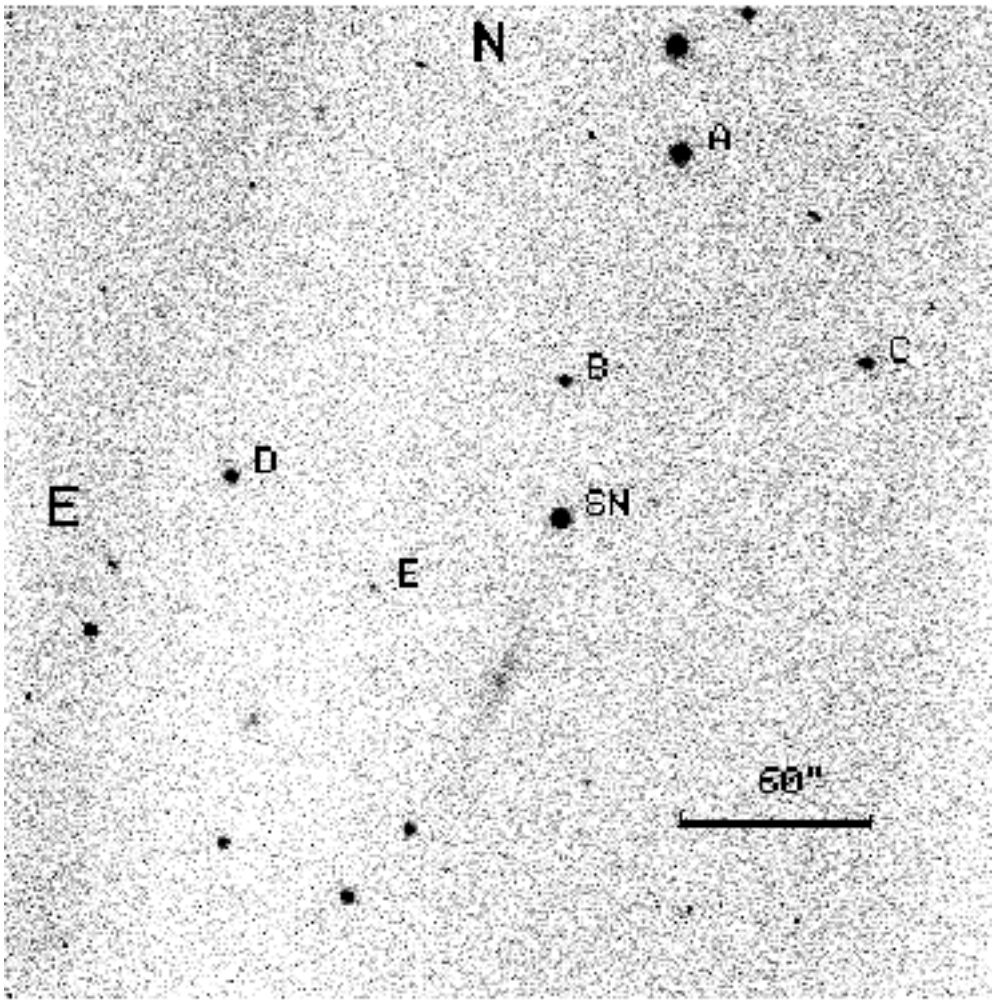
N
A
B
C
D
E
E
SN
60"

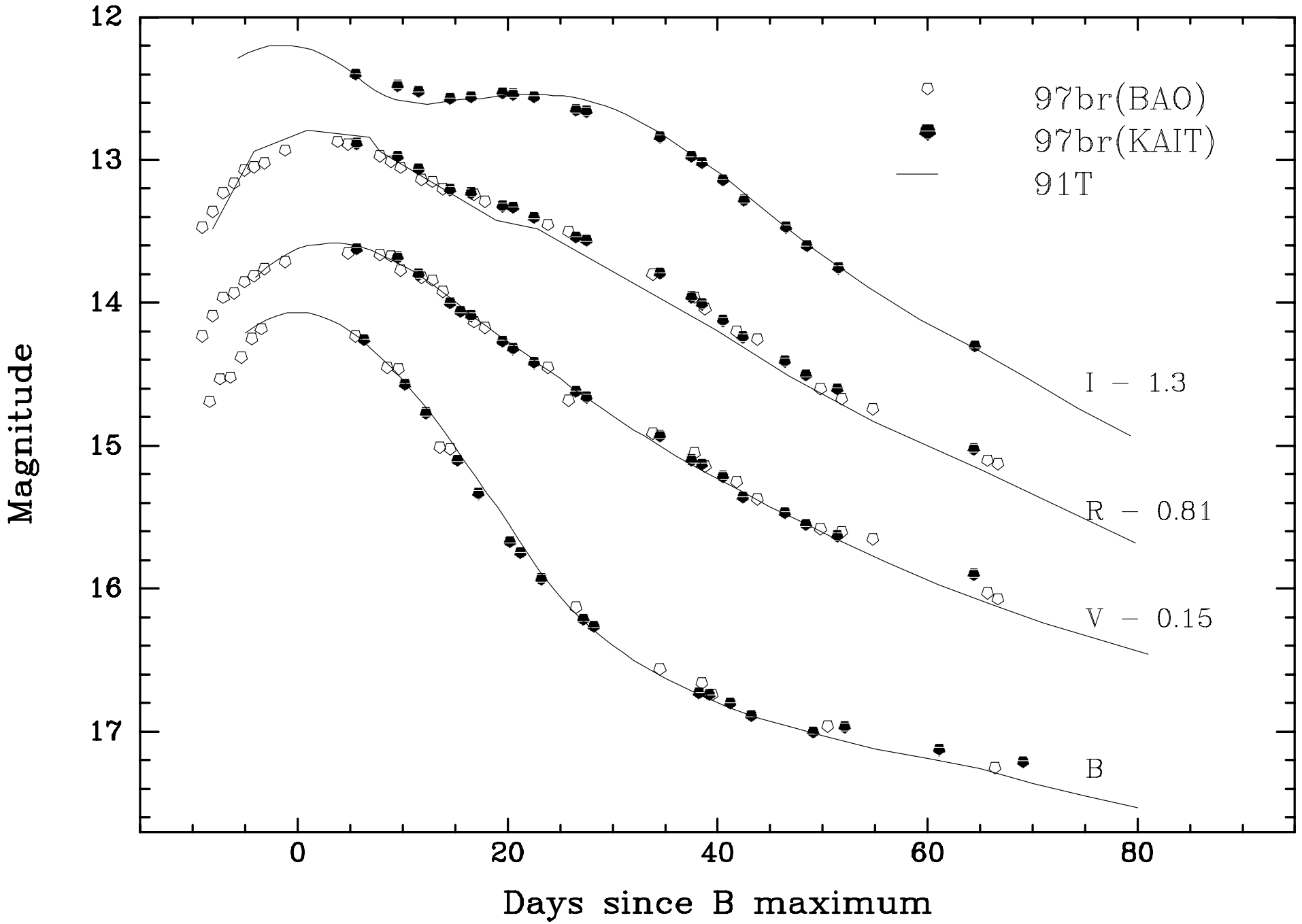
12
13
14
15
16
17
Magnitude
0
20
40
60
80
Days since B maximum
97br(BAO)
97br(KAIT)
91T
I − 1.3
R − 0.81
V − 0.15
B

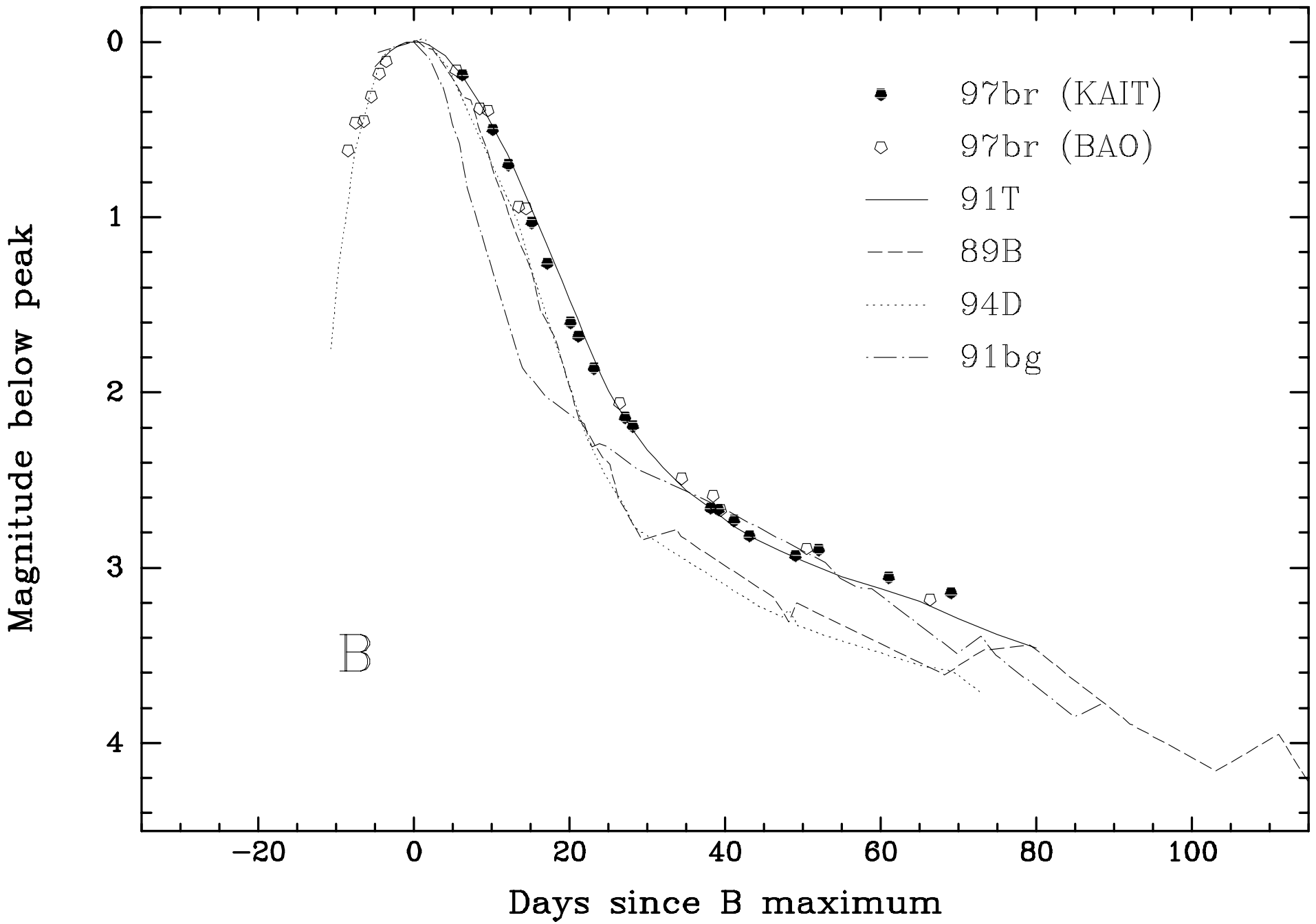
Magnitude below peak
Days since B maximum
B
97br (KAIT)
97br (BAO)
91T
89B
94D
91bg
0
1
2
3
4
−20
0
20
40
60
80
100

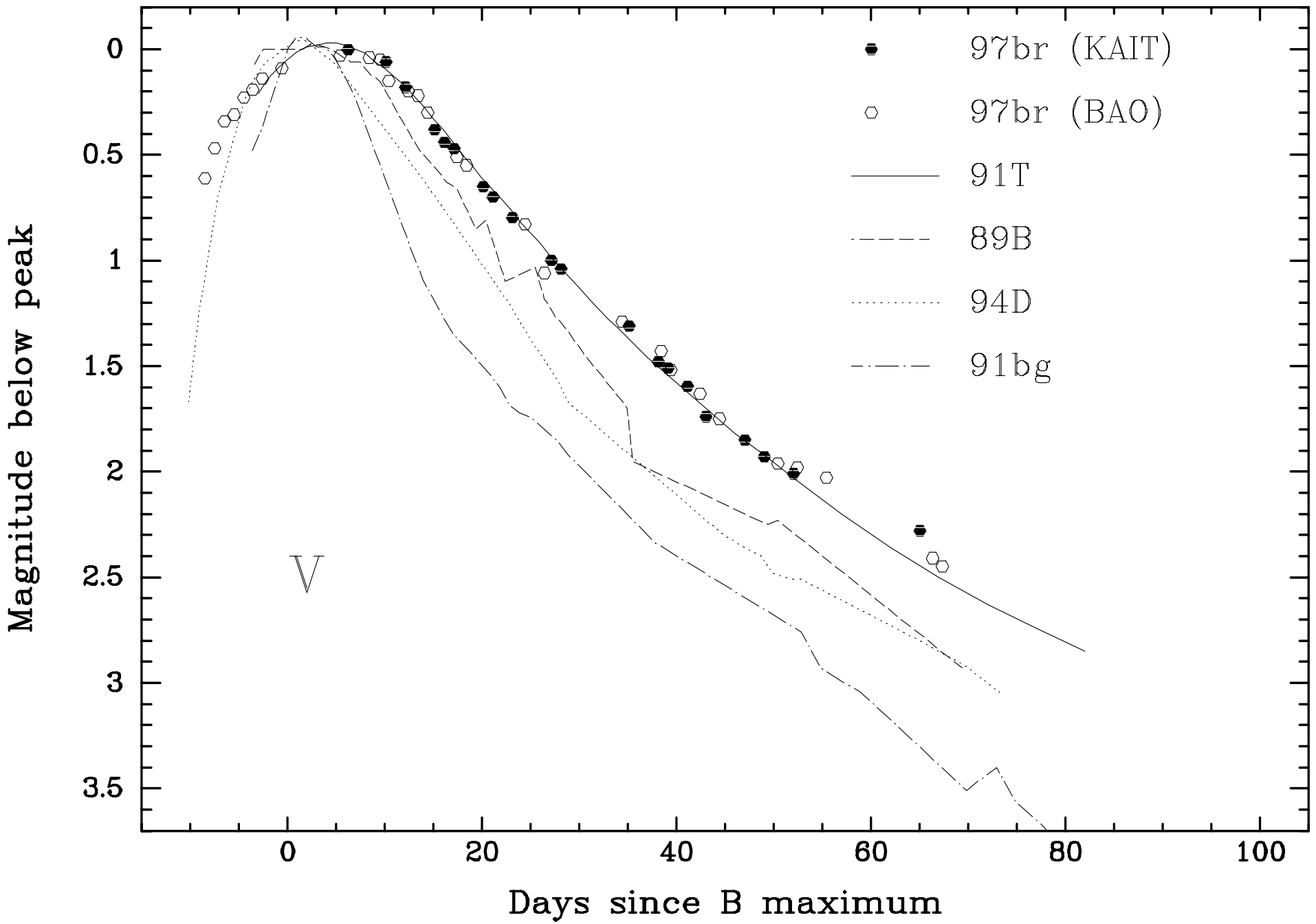
97br (KAIT)
97br (BAO)
91T
89B
94D
91bg
V
Magnitude below peak
Days since B maximum
0
0.5
1
1.5
2
2.5
3
3.5
0
20
40
60
80
100

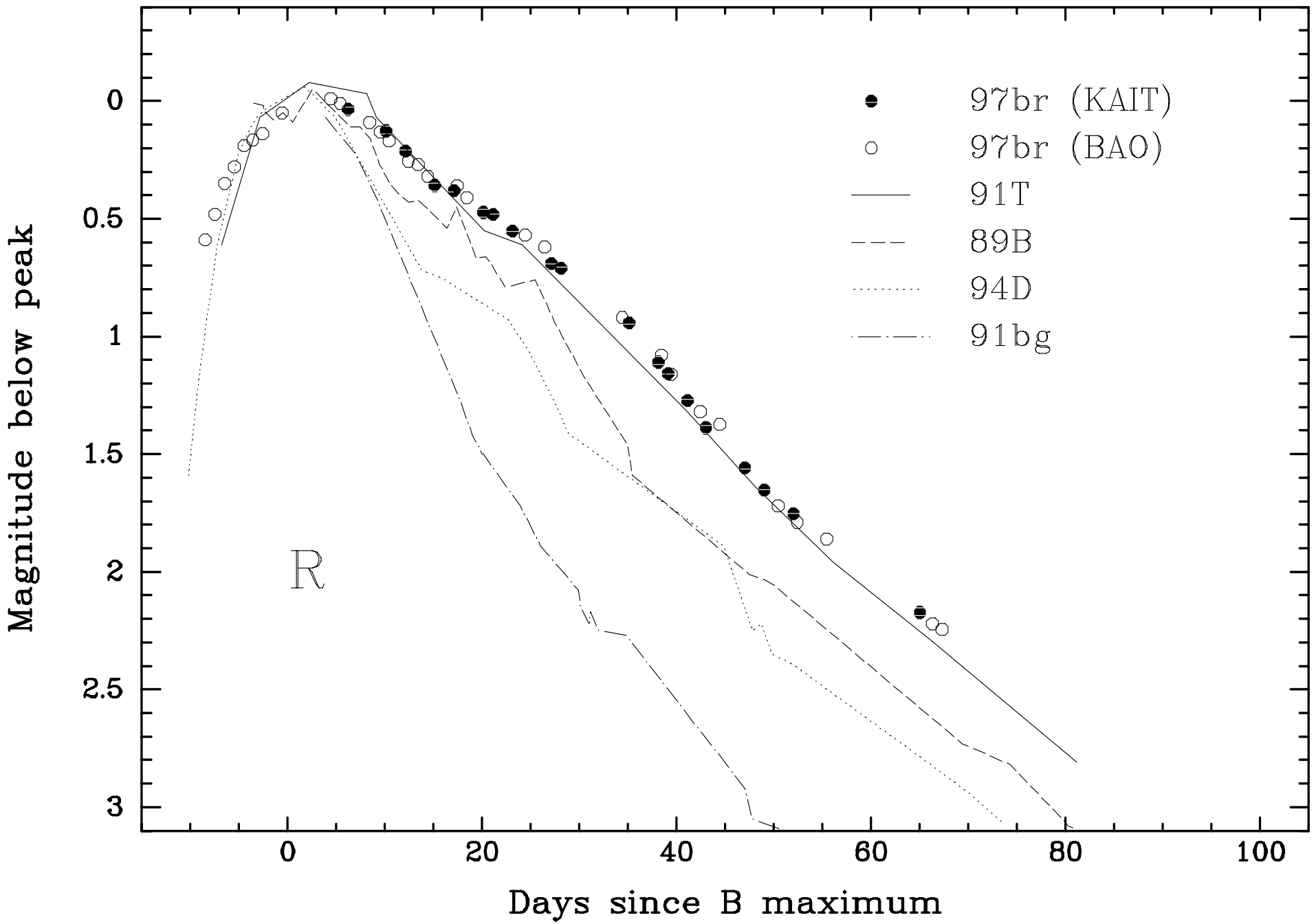
97br (KAIT)
97br (BAO)
91T
89B
94D
91bg
R
Magnitude below peak
Days since B maximum
0
0.5
1
1.5
2
2.5
3
0
20
40
60
80
100

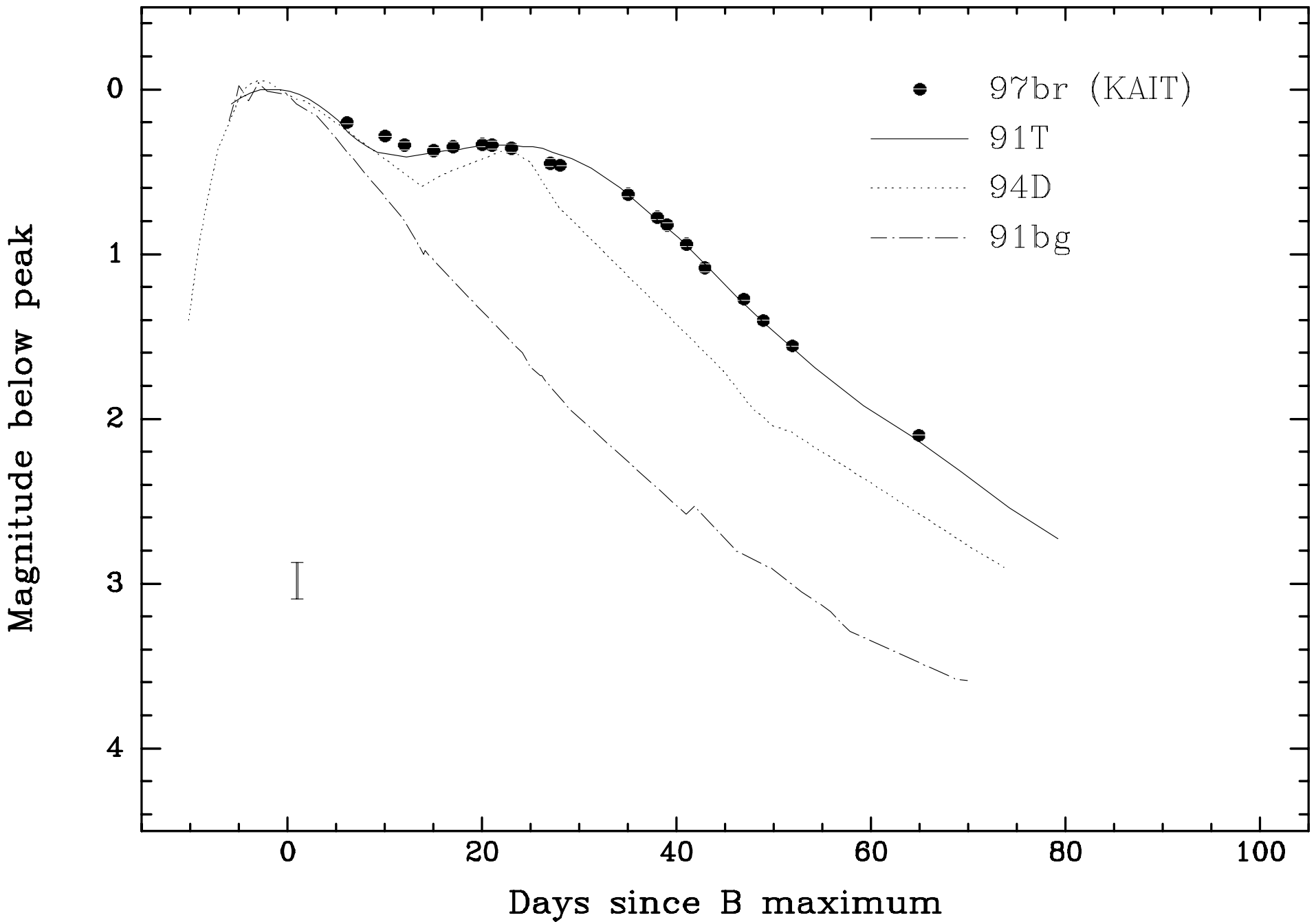
97br (KAIT)
91T
94D
91bg
Magnitude below peak
Days since B maximum
0
1
2
3
4
0
20
40
60
80
100

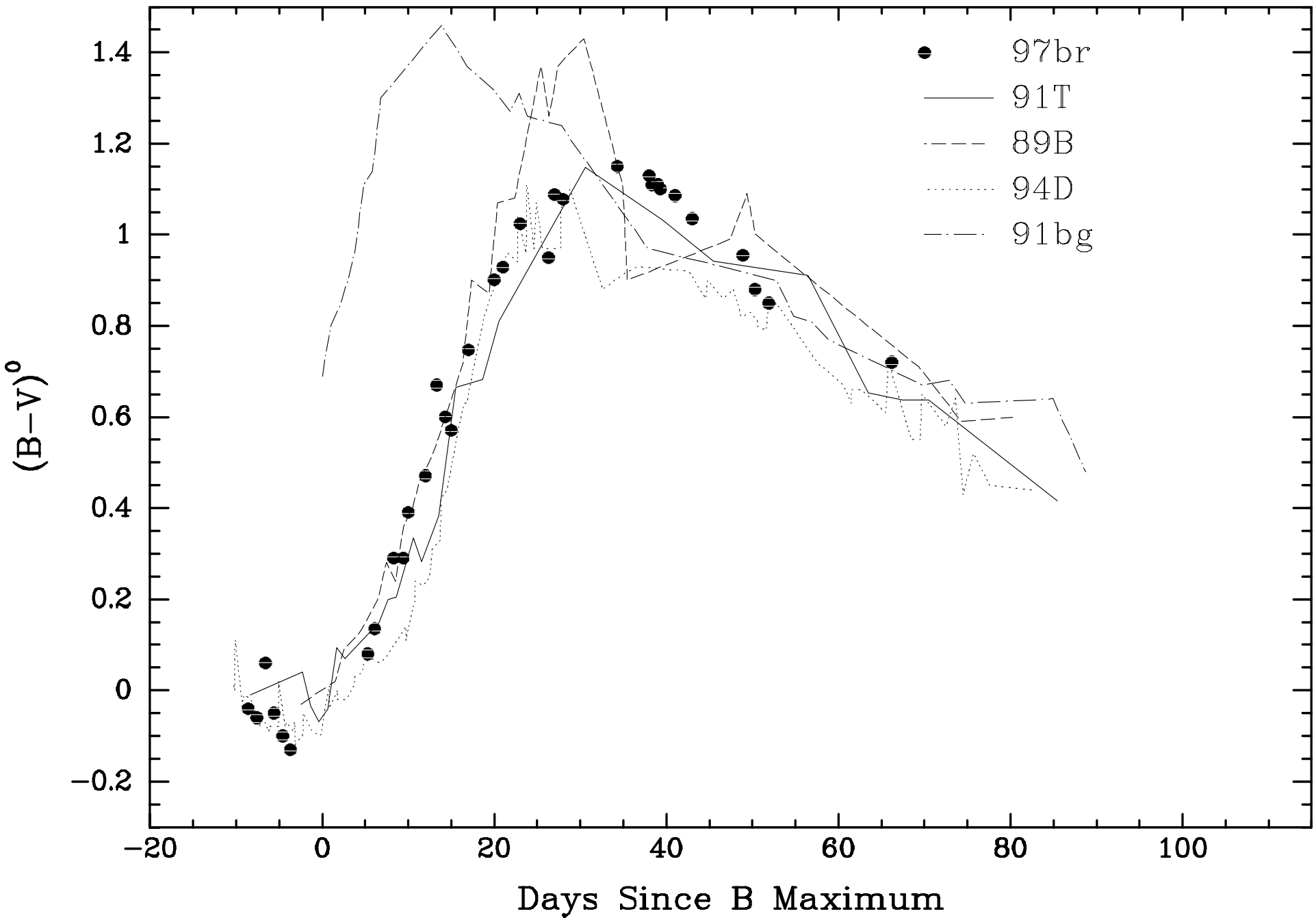
97br
91T
89B
94D
91bg
(B−V)°
Days Since B Maximum
1.4
1.2
1
0.8
0.6
0.4
0.2
0
−0.2
−20
0
20
40
60
80
100

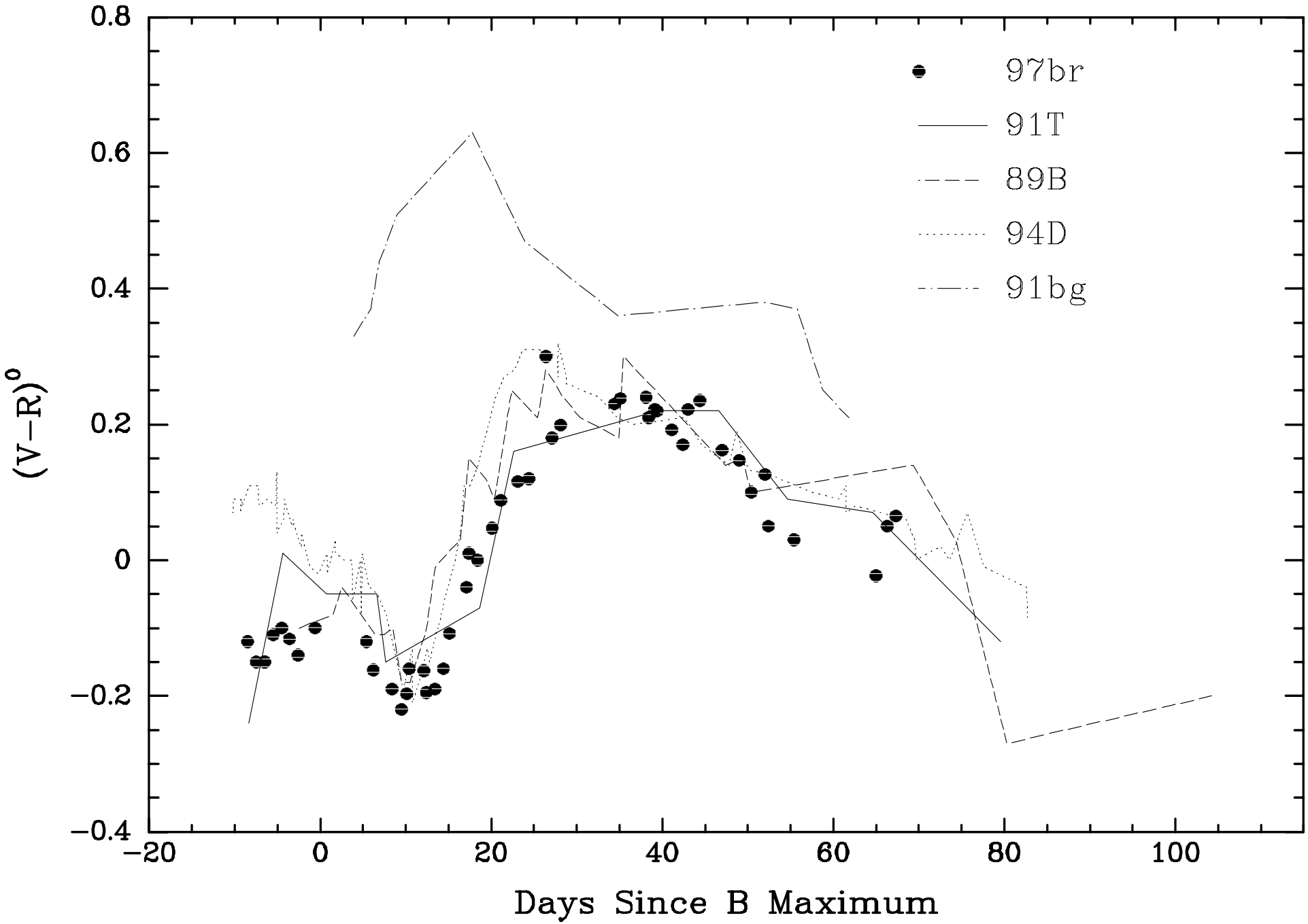
97br
91T
89B
94D
91bg
(V−R)°
Days Since B Maximum
0.8
0.6
0.4
0.2
0
−0.2
−0.4
−20
0
20
40
60
80
100

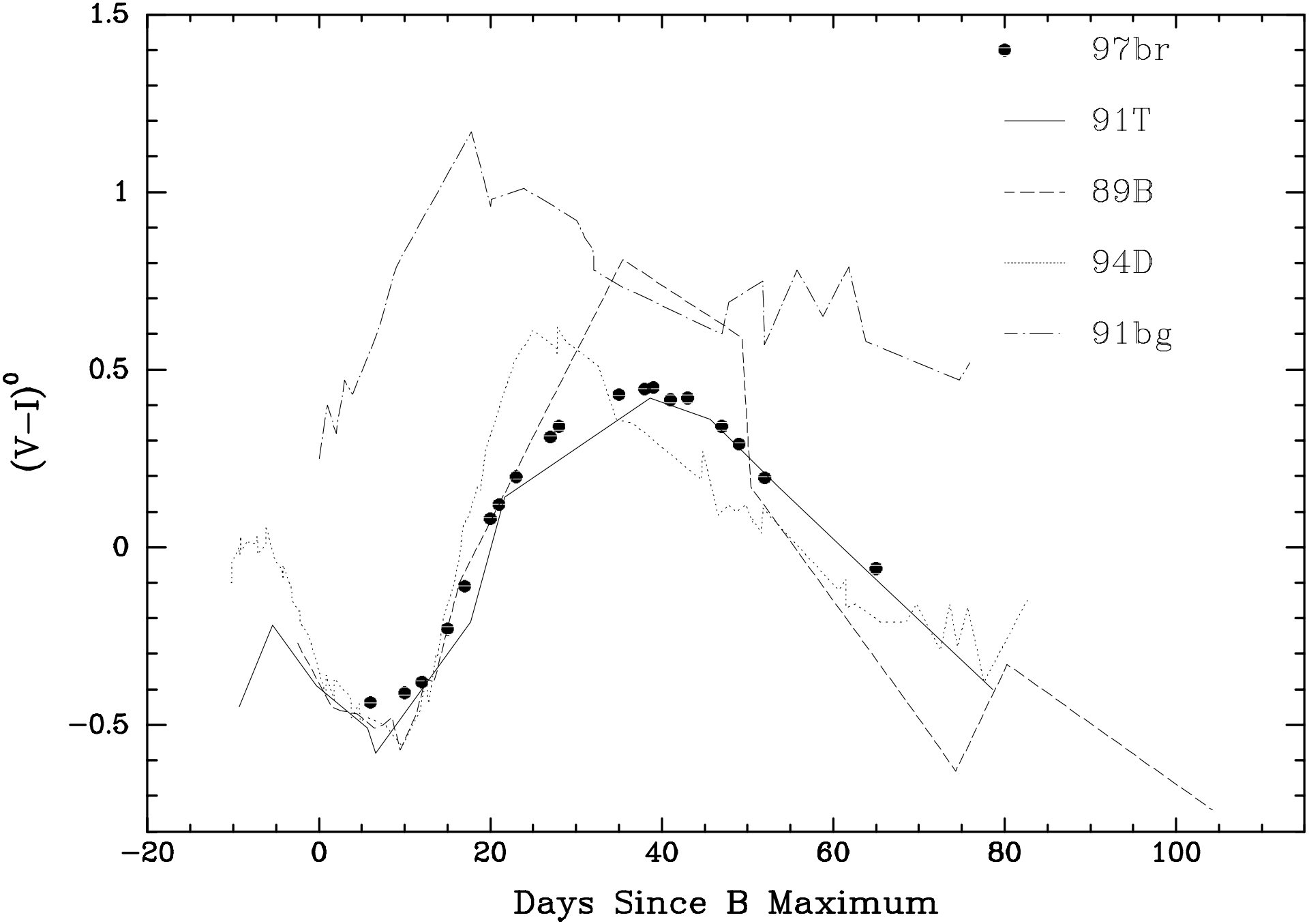
97br
91T
89B
94D
91bg
(V−I)°
Days Since B Maximum
1.5
1
0.5
0
−0.5
−20
0
20
40
60
80
100

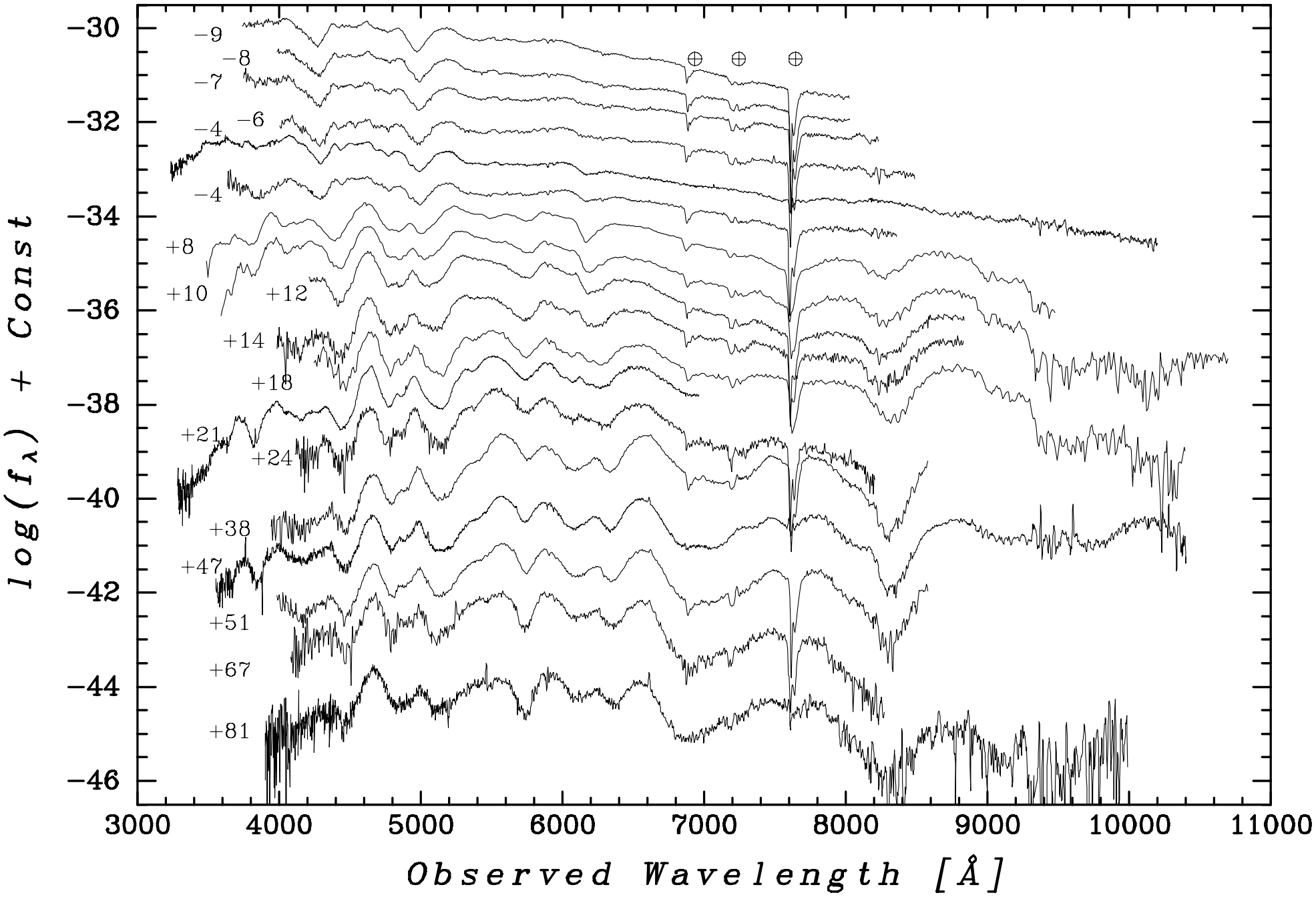
−9
−8
−7
−6
−4
−4
−4
+8
+10
+12
+14
+18
+21
+24
+38
+47
+51
+67
+81
⊕
⊕
⊕
−30
−32
−34
−36
−38
−40
−42
−44
−46
3000
4000
5000
6000
7000
8000
9000
10000
11000
log(f_λ) + Const
Observed Wavelength [Å]

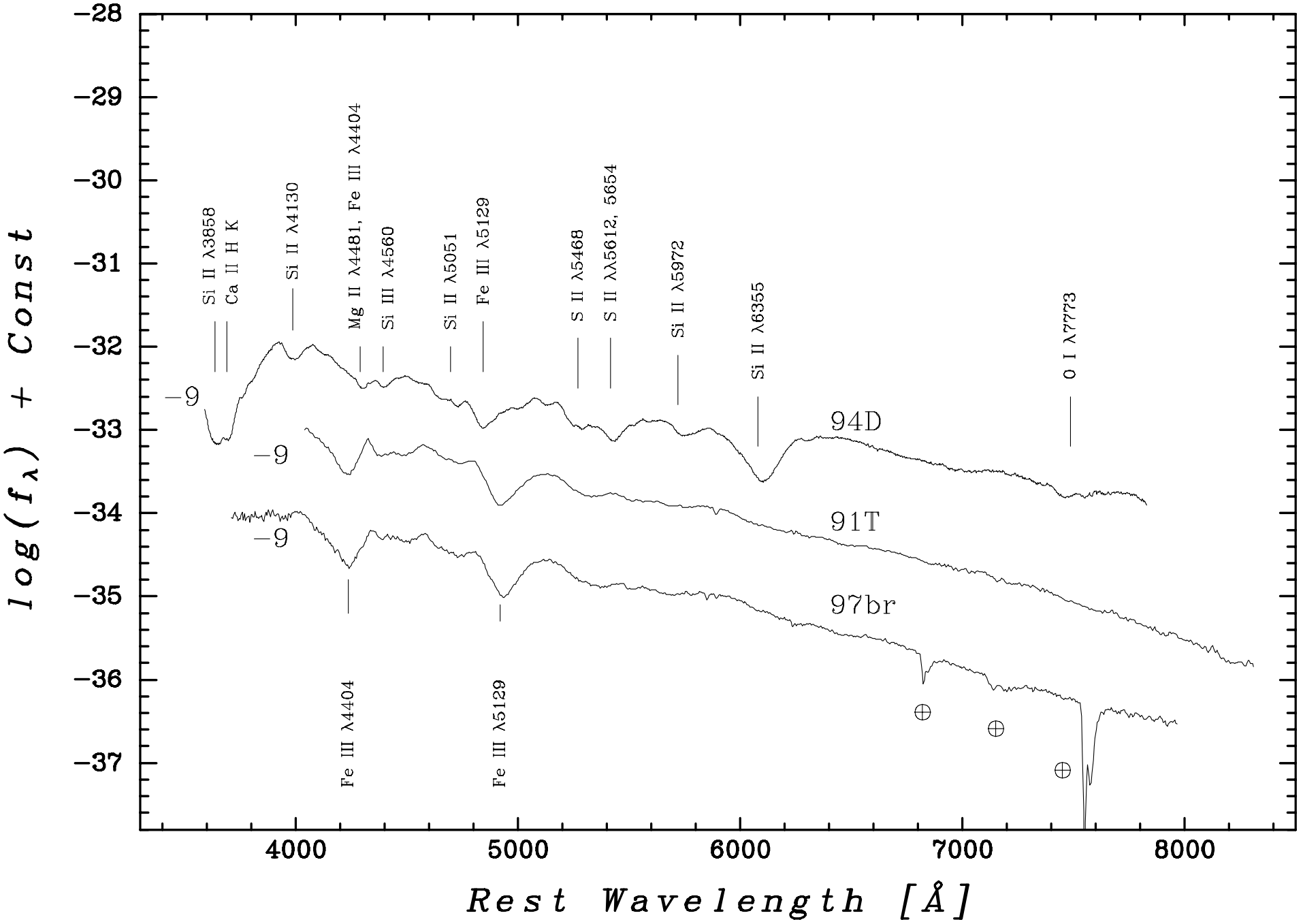
log(f_λ) + Const
Rest Wavelength [Å]
−28
−29
−30
−31
−32
−33
−34
−35
−36
−37
4000
5000
6000
7000
8000
Si II λ3858
Ca II H K
Si II λ4130
Mg II λ4481, Fe III λ4404
Si III λ4560
Si II λ5051
Fe III λ5129
S II λ5468
S II λλ5612, 5654
Si II λ5972
Si II λ6355
O I λ7773
−9
94D
−9
91T
−9
97br
Fe III λ4404
Fe III λ5129
⊕
⊕
⊕

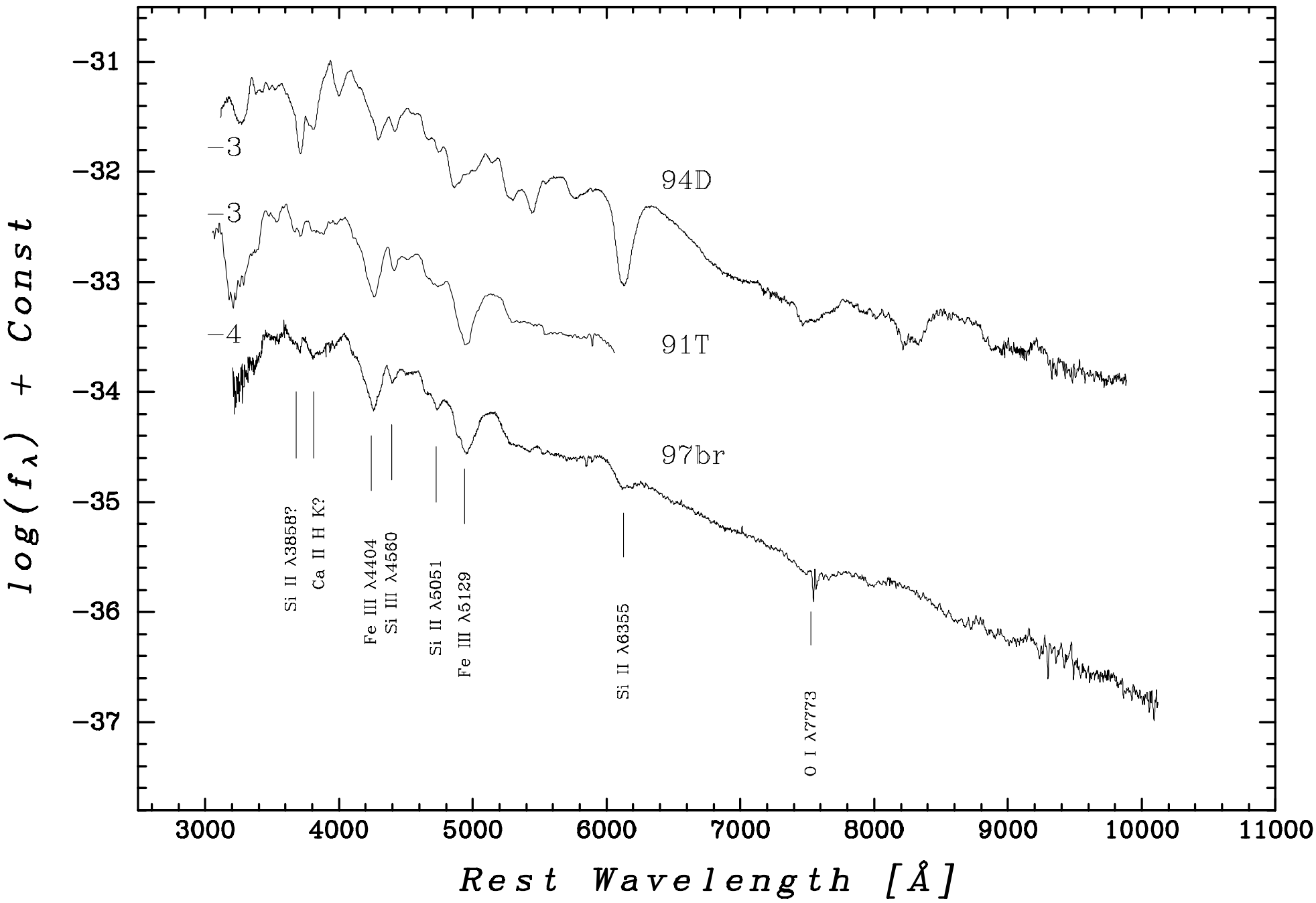
log(f_λ) + Const
Rest Wavelength [Å]
−31
−32
−33
−34
−35
−36
−37
3000
4000
5000
6000
7000
8000
9000
10000
11000
−3
−3
−4
94D
91T
97br
Si II λ3858?
Ca II H K?
Fe III λ4404
Si III λ4560
Si II λ5051
Fe III λ5129
Si II λ6355
O I λ7773

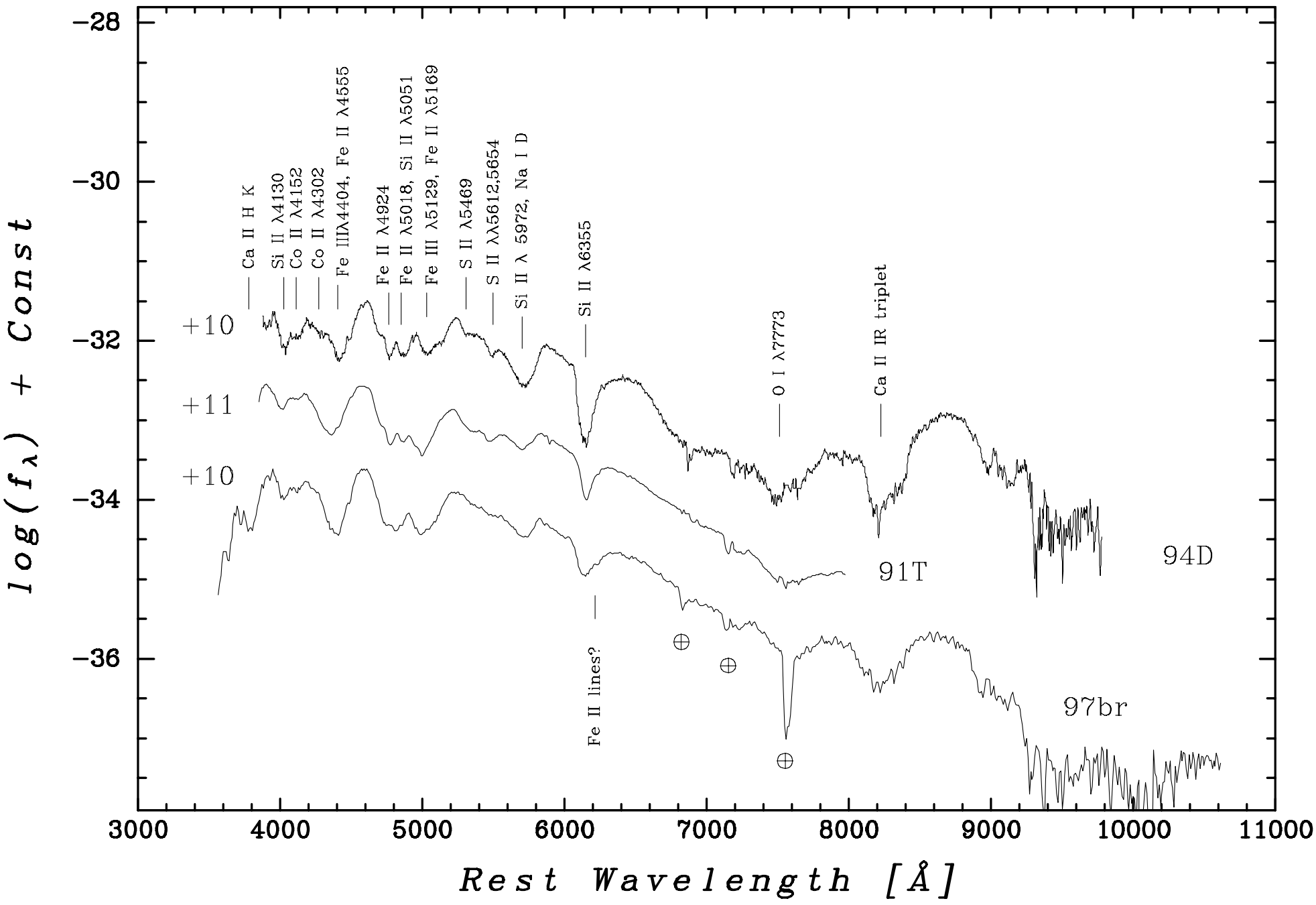
log(f_λ) + Const
Rest Wavelength [Å]
−28
−30
−32
−34
−36
3000
4000
5000
6000
7000
8000
9000
10000
11000
Ca II H K
Si II λ4130
Co II λ4152
Co II λ4302
Fe III λ4404, Fe II λ4555
Fe II λ4924
Fe II λ5018, Si II λ5051
Fe III λ5129, Fe II λ5169
S II λ5469
S II λλ5612,5654
Si II λ 5972, Na I D
Si II λ6355
O I λ7773
Ca II IR triplet
Fe II lines?
+10
+11
+10
94D
91T
97br
⊕
⊕
⊕

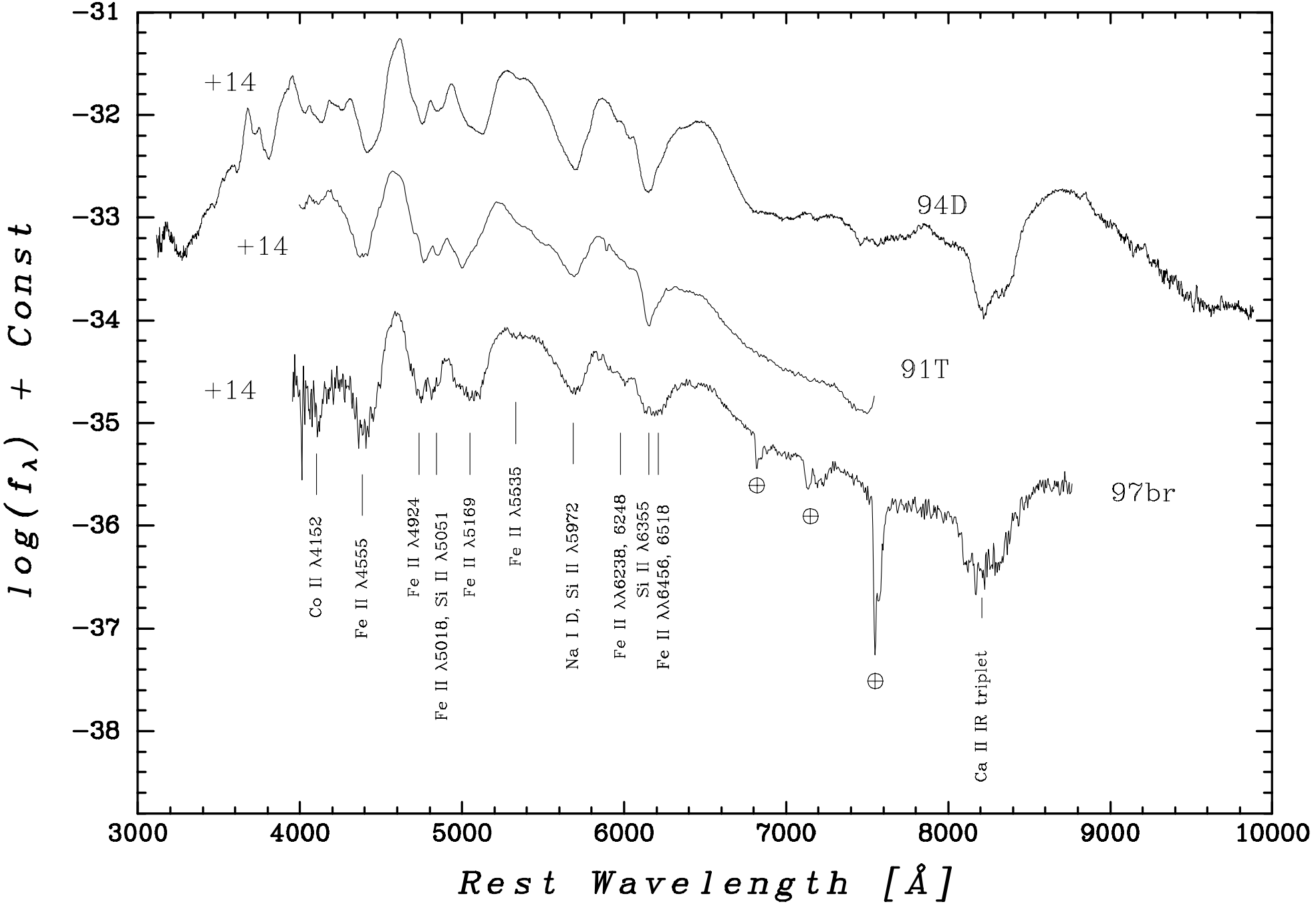
log(f_λ) + Const
Rest Wavelength [Å]
+14
+14
+14
94D
91T
97br
Co II λ4152
Fe II λ4555
Fe II λ4924
Fe II λ5018, Si II λ5051
Fe II λ5169
Fe II λ5535
Na I D, Si II λ5972
Fe II λλ6238, 6248
Si II λ6355
Fe II λλ6456, 6518
Ca II IR triplet
⊕
⊕
⊕
−31
−32
−33
−34
−35
−36
−37
−38
3000
4000
5000
6000
7000
8000
9000
10000

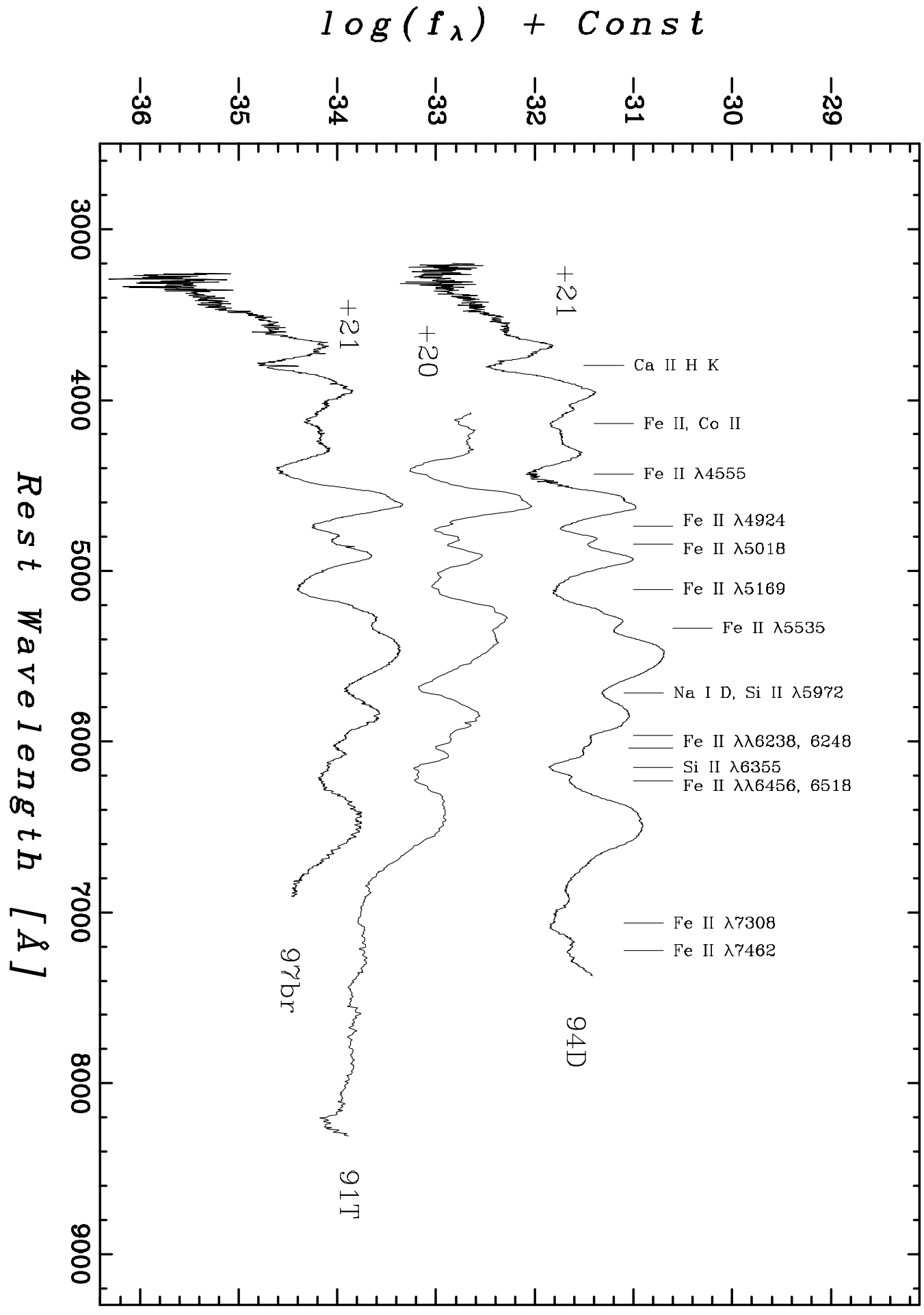
log(f_λ) + Const
−36
−35
−34
−33
−32
−31
−30
−29
3000
4000
5000
6000
7000
8000
9000
Rest Wavelength [Å]
+21
+20
+21
+21
Ca II H K
Fe II, Co II
Fe II λ4555
Fe II λ4924
Fe II λ5018
Fe II λ5169
Fe II λ5535
Na I D, Si II λ5972
Fe II λλ6238, 6248
Si II λ6355
Fe II λλ6456, 6518
Fe II λ7308
Fe II λ7462
97br
94D
91T

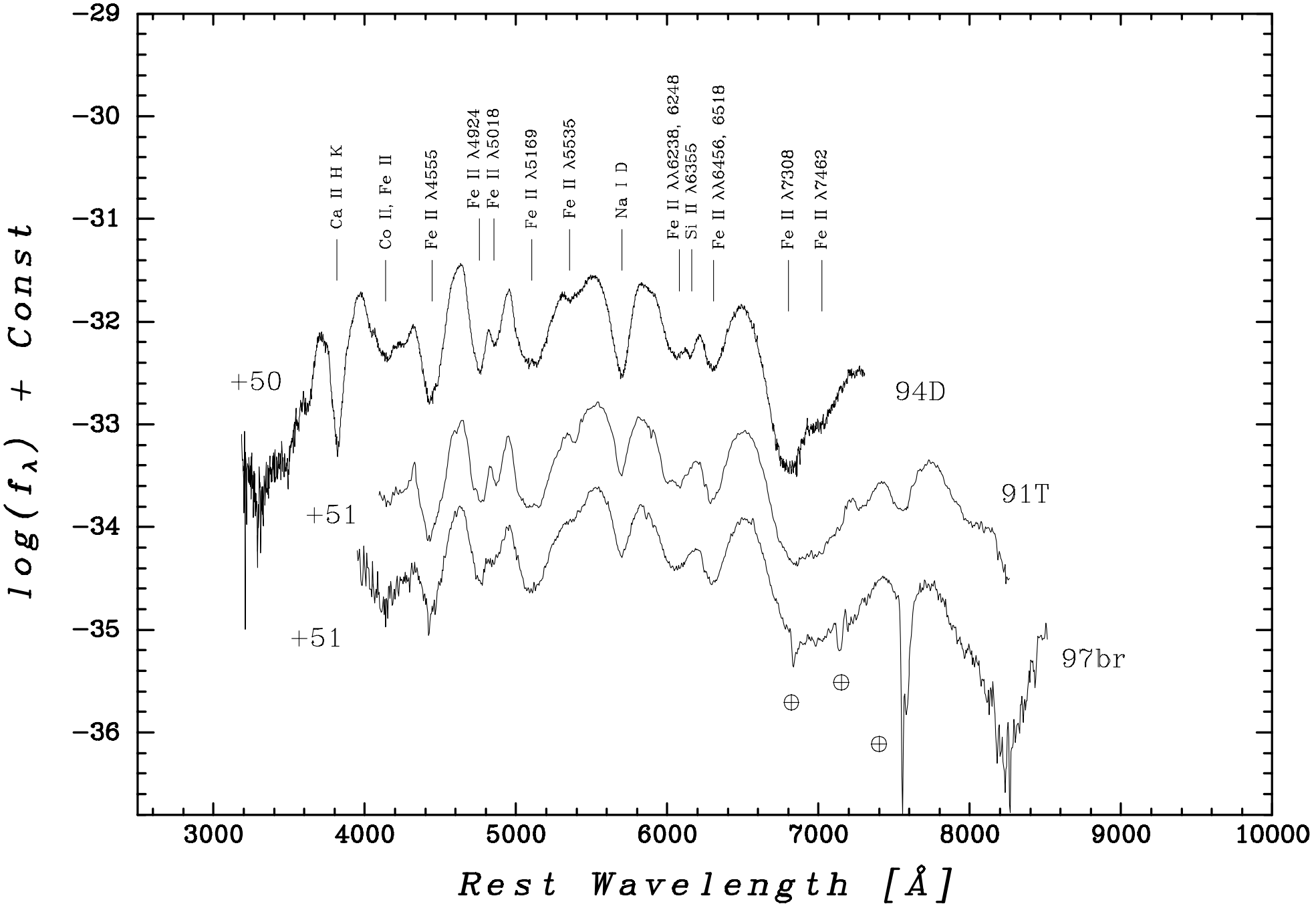
log(f_λ) + Const
Rest Wavelength [Å]
−29
−30
−31
−32
−33
−34
−35
−36
3000
4000
5000
6000
7000
8000
9000
10000
Ca II H K
Co II, Fe II
Fe II λ4555
Fe II λ4924
Fe II λ5018
Fe II λ5169
Fe II λ5535
Na I D
Fe II λλ6238, 6248
Si II λ6355
Fe II λλ6456, 6518
Fe II λ7308
Fe II λ7462
+50
94D
+51
91T
+51
97br
⊕
⊕
⊕

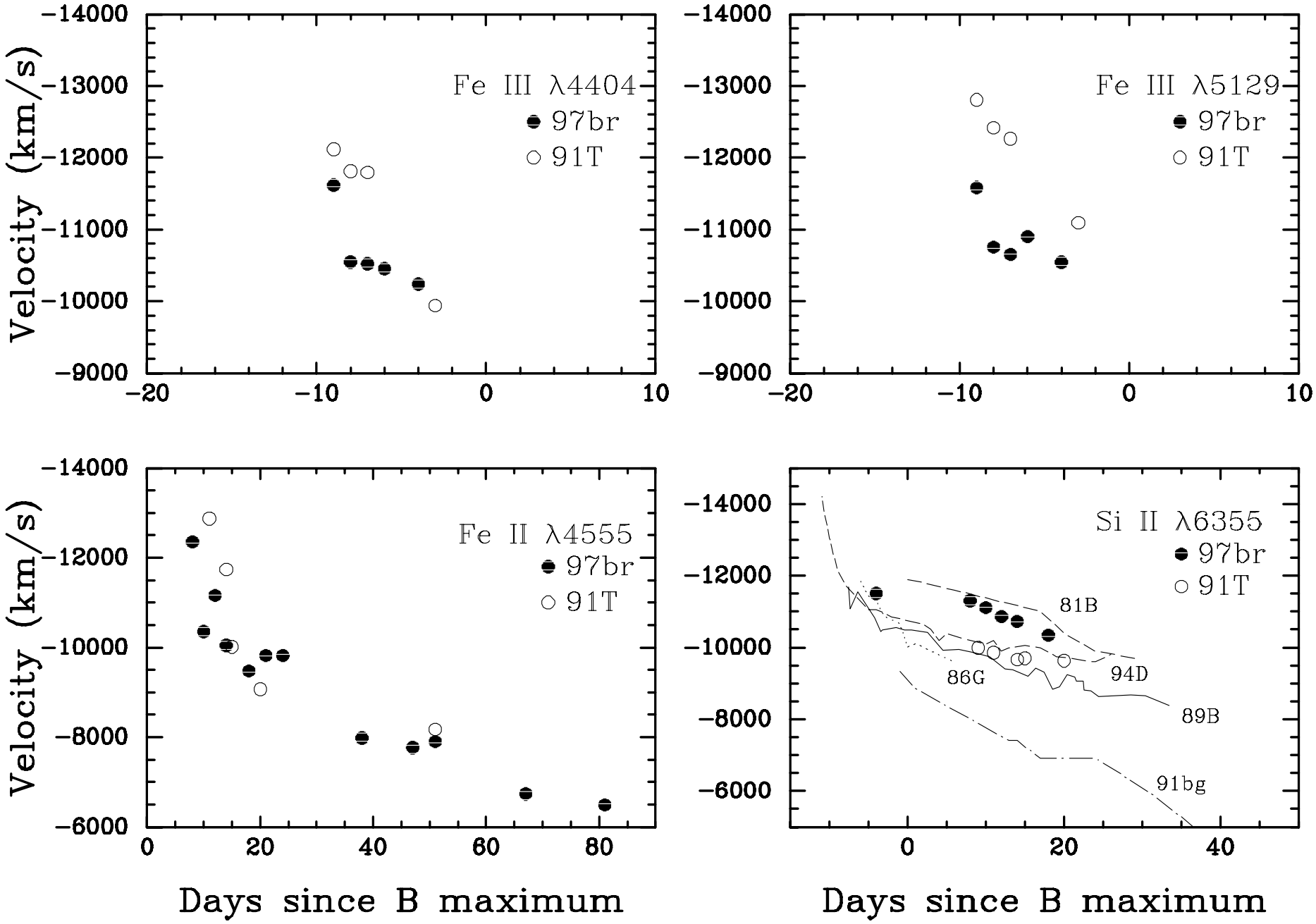
Velocity (km/s)
Fe III λ4404
97br
91T
Fe III λ5129
97br
91T
Fe II λ4555
97br
91T
Si II λ6355
97br
91T
81B
86G
94D
89B
91bg
Days since B maximum
Days since B maximum

arXiv:astro-ph/9903466v1 30 Mar 1999

The Type Ia Supernova 1997br in ESO576-G40

W.D. Li[1,2], Y.L. Qiu[1], Q.Y. Qiao[1], X.H. Zhu[1], J.Y. Hu[1],
M.W. Richmond[3], A.V. Filippenko[2], R.R. Treffers[2], C.Y. Peng[4], D.C. Leonard[2]

[1] Beijing Astronomical Observatory, Chinese Academy of Sciences, Zhongguancun Beijing, 100080, P. R. China

[2]Department of Astronomy, University of California, Berkeley, CA 94720-3411

[3]Department of Physics, Rochester Institute of Technology, Rochester, NY 14623

[4]Department of Astronomy, University of Arizona, AZ 85721

Received _____; accepted _____

ABSTRACT

The peculiar type Ia supernova SN 1997br in ESO576-G40 was extensively observed at Beijing Astronomical Observatory (BAO) and Lick Observatory. In this paper, we present and discuss the $BVRI$ photometry and the spectra collected over three months, starting from 9 days before maximum brightness.

The light curves of SN 1997br are similar to those of SN 1991T, with slow decline rates after the B maximum. Well sampled data before the B maximum show unambiguously that SN 1997br rises more slowly and has a wider peak than normal type Ia supernovae. The optical color evolution of SN 1997br is also similar to that of SN 1991T. We estimate the extinction of SN 1997br to be $E(B-V)$=0.35±0.10 by comparing its $BVRI$ light curves to those of SN 1991T and by measuring the equivalent width of interstellar Na I D absorption lines.

We have conducted a thorough comparison of the spectroscopic evolution of SN 1997br, SN 1991T, and SN 1994D. Although SN 1997br is generally very similar to SN 1991T, it shows some interesting differences at various epochs. Spectra of SN 1997br seem to indicate an earlier transition to the dominant phase of Fe peak elements after the B maximum. Si II lines in SN 1997br show a very short duration after the B maximum.

We discuss the implications of our observations of SN 1997br for models of type Ia supernovae. Specifically, we suggest that some SNe Ia may result from decelerated detonations of white dwarfs.

Subject headings: supernovae: general – supernovae: individual (SN 1997br)

1. Introduction

SN 1997br in ESO576-G40 was discovered by the BAO Supernova (SN) Survey in an image taken on 1997 Apr 10.6 UT (Li et al. 1997a; Li 1997), the twelfth supernova to be discovered by the BAO SN survey since its inception in early 1996. A low resolution optical spectrum obtained shortly after the discovery (Qiao et al. 1997a) identified the event as a peculiar SN 1991T-like type Ia, with prominent Fe III absorption lines superimposed on a rather blue continuum. Li et al. (1997a) measured an accurate position for SN 1997br as α = 13h20m42.s40, δ = -22^{o}02'12."3 (equinox J2000.0), which is 20.6" west and 51.6" north of the nucleus of ESO576-G40. A follow-up program of multicolor photometry and spectroscopy was immediately established at BAO for this peculiar supernova. Numerous observations were also obtained at Lick Observatory. We report here on the results from the first 90 days after discovery.

Section 2 contains a description of the observations and analysis of the photometry: our methods of performing photometry, our calibration of the measurements onto the standard Johnson-Cousins system, our resulting multicolor light curves, and our comparison between the light curves of SN 1997br, SN 1991T, and other type Ia supernovae (SNe Ia). Section 3 contains a description of the observations and analysis of the spectra of SN 1997br. The good temporal coverage of the spectral observations (17 spectra from 9 days before to 81 days after B maximum) enables us to monitor the evolution of many features. A through comparison is done between the spectra of SN 1997br, SN 1991T, and the normal SN Ia 1994D. We discuss the implications of our observations in Section 4 and summarize our conclusions in Section 5.

2. Photometry

2.1. Observations and data reduction

Broadband $BVRI$ images of SN 1997br were obtained using CCD detectors on the BAO 0.6m telescope and the Lick 0.76m Katzman Automatic Imaging Telescope (KAIT) beginning the second day after discovery and continuing for about 90 days. The BAO observations were made at the f/4.23 prime focus using a TI 1024×1024 pixel CCD (0.96 arcsec pixel^{-1}); only BVR filters were used due to a shortage of positions on the filter wheel (the position of the I filter was occupied by a clear filter for the BAO SN survey). The KAIT images ($BVRI$) were taken at the f/8.17 Cassegrain focus using a Tektronix 512×512 pixel CCD (0.63 arcsec pixel^{-1}). Calibration of the field was done at BAO on 1997 Jun 14 by observing Landolt (1992) standards at different airmass throughout the night, but reduction of the data suggests that conditions might not have been photometric. Another calibration of the field came from observations made by Ricardo Covarrubias of CTIO, who used the CTIO 0.91m telescope on 1997 May 3, and we adopt it throughout this paper.

Instrumental magnitudes for the standards were measured using the IRAF DAOPHOT package and then used to determine transformation coefficients to the standard systems of Johnson (Johnson et al. 1966; for BV) and Cousins (Cousins 1981; for RI). The derived transformation coefficients and color terms were used to calibrate a sequence of five stars near SN 1997br. Figure 1 shows a KAIT image of SN 1997br, with the SN and the five local standard stars marked. The magnitudes of these five stars and the associated uncertainties are listed in Table 1. Star E is rather faint and did not always appear on all images.

Measuring the brightness of SNe is usually complicated by the background surface brightness of their host galaxies, necessitating template subtraction (e.g., Hamuy et al. 1994; Richmond et al. 1995). In the case of SN 1997br, however, the measurement is relatively straightforward: the SN is 55.6 arcsec from the nucleus of its host galaxy, in a faint region of the host galaxy. We could have used simple aperture photometry to measure the magnitudes of the SN and the comparison stars, but we instead adopt the more sophisticated point spread function (PSF) fitting method for the following reasons: (1) Although the typical FWHM is about 3-4 pixels in the BAO and KAIT images, some images have FWHM larger than 8 pixels, in which case PSF fitting is superior. We choose to use the same method for all our images to ensure that the results are obtained in a consistent manner. (2) There are many bright, isolated stars with which to define the PSF. (3) The PSF fitting method creates an image with stars subtracted, from which we can estimate whether the brightness of the SN is measured correctly.

Schmidt et al. (1993) found that the PSF fitting method can systematically overestimate or underestimate the brightness of an object when there is a strong gradient in the background, but the errors can be reduced substantially by using only the inner core of an object to fit the PSF. Though we don't have a strong gradient in the background of SN 1997br, we choose to adopt this procedure and set our fitting radius of the PSF to be the value of FWHM. Using only the inner core to fit the PSF also yields higher signal-to-noise ratios when performing differential photometry between the SN and the local standard stars.

To measure the sky background of the SN, we always use an annulus with radii 15-20 pixels (14.4"-19.2" for BAO images, 9.45"-12.6" for KAIT images), thereby avoiding possible substantial variations in the host galaxy light near the SN. For local standard stars, on the other hand, we use an annulus with radius (4-5)×FWHM (typically 14-20 pixels) to measure the sky background.

The instrumental magnitudes measured from this PSF fitting method are transformed onto the standard Johnson-Cousins system. For the BAO observations, the color terms of the filters are determined from calibration observations obtained in Dec 1995 and Jan 1996 and are of the following form:

$$V = v - 0.014(b - v) + C_V,$$

$$(B - V) = 1.19(b - v) + C_{BV},$$

$$(V - R) = 0.91(v - r) + C_{VR}.$$

Here, capital letters denote magnitudes in the standard system and lower-case letters denote instrumental magnitudes. The terms C_V, C_{BV} and C_{VR} are the differences between the zero points of the instrumental and standard magnitudes, which can vary from night to night. Since we always measure the magnitudes of SN 1997br relative the those of several local comparison stars, these terms are not involved in the photometric solutions. The color terms for the KAIT observations are determined from calibration observations obtained on Jun 14, 15, and 18, 1998 and are of the following form:

$$V = v - 0.005(b - v) + C_V,$$

$$(B - V) = 1.12(b - v) + C_{BV},$$

$$(V - R) = 0.83(v - r) + C_{VR},$$

$$(V - I) = 0.95(v - i) + C_{VI}.$$

Our final results of the CCD photometry are listed in Table 2, and our $BVRI$ light curves for SN 1997br are shown in Figure 2 together with the best χ^2-minimizing fits to those of SN 1991T (Hamuy et al. 1996a for BVI; Ford et al. 1993 for R). From these fits we can see that the photometric behavior of SN 1997br is very similar to that of SN 1991T. After calculating the times and magnitudes at peak, we will discuss each light curve in turn, comparing it with those of other type Ia SNe.

2.2. Optical light curves

The times and magnitudes of the peak in each filter are listed in Table 3. Unfortunately, there are large gaps near the maxima of these light curves (especially B) because of poor weather and the proximity of the SN to the bright moon, so these parameters cannot be measured directly. In order to determine these values we use two methods: (1) fit a cubic spline function to the BVR light curves (spline fitting), and (2) fit the $BVRI$ light curves of SN 1991T to those of SN 1997br (template fitting). Note that the second method is the only way to get an estimate of the time and peak of the I-band light curve since we have no pre-maximum observations. We prefer to adopt the results of spline fitting for the R-band light curve, since the SN 1991T template is not a detailed match to the SN 1997br data and gives a peak 0.08 mag brighter. Measurements for the B and V light curves from the two methods are consistent with each other within the uncertainties, so we average them to give the results in Table 3.

In Figures 3-6, we compare the light curves of SN 1997br with those of several other well-observed SNe Ia: SN 1991T (Hamuy et al. 1996a for BVI; Ford et al. 1993 for R); SN

1989B (Wells et al. 1994); SN 1994D (Richmond et al. 1995), and SN 1991bg (Filippenko et al. 1992b; Leibundgut et al. 1993). All light curves are shifted in times and peak magnitudes to match those of SN 1997br.

The B-band light curve of SN 1997br (Fig. 3) is similar to, but seems to decline faster than that of SN 1991T. Following Phillips (1993) and Hamuy et al. (1996a), we define $\Delta m_{15}(X)$ as the difference between the magnitude at peak and 15 days after the peak in the X passband, and measure $\Delta m_{15}(B) = 1.00 \pm 0.15$ for SN 1997br. The uncertainty, which is somewhat large due to our lack of observations around the peak, is the sum in quadrature of the uncertainty in the B-band peak magnitude, the change in the interpolated magnitude 15 days after peak if the date of maximum is changed by the amount listed in Table 3, and the uncertainty of the observed magnitudes. This $\Delta m_{15}(B)$ value of SN 1997br is larger than that of SN 1991T (0.94 ± 0.07), but smaller that that of SN 1989B (1.31 ± 0.07), SN 1994D (1.28 ± 0.05), and SN 1991bg (1.88 ± 0.10), and is at the lower end of the distribution of $\Delta m_{15}(B)$ for all SNe Ia in the Calán/Tololo Supernova Survey (Hamuy et al. 1996b). The decline rate of SN 1997br changes at about 30 days past maximum and is nearly the same as that of SN 1991T thereafter.

The behavior of such a 1991T-like type Ia SN is obtained with good quality CCD measurements at a very early phase (9 days before B maximum). These premaximum observations of SN 1997br show unambiguously that it rises more slowly than normal SNe Ia such as SN 1994D and may have a larger rise time from explosion to B maximum. The width of the peak at 0.6 mag below maximum is about 20 days for SN 1997br, while it is about 17 days for SN 1994D.

In the V band (Fig. 4), the peak width of SN 1997br is again similar to that of SN 1991T, and is wider than that of SN 1994D, SN 1989B, and SN 1991bg. The V light curve of SN 1997br displays a wide, flat-topped feature around it maximum, within 0.05 of the peak for more than 10 days. Using the definition of Δm_{15} above, we measured $\Delta m_{15}(V)$=0.57 ± 0.08 for SN 1997br, which is similar to that of SN 1991T (0.59 ± 0.06) and smaller than that of SN 1994D (0.76 ± 0.04) and SN 1989B (0.71 ± 0.07).

We show the R band light curve in Fig. 5, in which SN 1997br begins to deviate strongly from a simple decline after B maximum. From 13 to 44 days after B maximum,the R-band light curve develops a prominent "shoulder" seen in most other well-observed SNe Ia in the R-band (Ford et al. 1993; Wells et al. 1994) except SN 1991bg. After this the curve declines at a constant rate of about 0.04 mag per day. SN 1997br shows a wider peak in the R band than do SN 1994D, SN 1989B, and SN 1991bg, and a longer duration "shoulder" than do SN 1994D and SN 1989B. The fit to the R-band light curve of SN 1991T is not so good, in part because the light curve of SN 1991T is not well-sampled. In particular, the lack of a "shoulder" in the R light curve of SN 1991T is due to a paucity of observations at the period.

Our I-band light curve of SN 1997br is shown in Fig. 6. Unfortunately there aren't

I-band observations at BAO, and the I-band observations from KAIT only began 6 days after the B maximum, so we are unable to directly measure the time and magnitude of the I-band peak. An estimate is done by fitting the I-band light curve of SN 1991T to that of SN 1997br; this yields the values listed in Table 3. From the fit we can see that the photometric behavior of SN 1997br in the I-band is almost the same as that of SN 1991T over the period of overlap. Unlike SN 1994D, which displays a pronounced dip at about 14 days after B maximum and a secondary peak about 23 days after B maximum, SN 1997br and SN 1991T show less obvious minima and secondary maxima; instead, there is a nearly constant plateau in I-band magnitude from about 14 to 24 days after B maximum.

In summary, the light curves of SN 1997br closely resemble those of SN 1991T, and differ significantly from those of normal SNe Ia such as SN 1994D and SN 1989B. The well-sampled premaximum light curves of SN 1997br unambiguously show that it rises and declines more slowly than do normal SNe Ia, and thus has wider peaks in the BVR passbands.

2.3. Optical color curves

We present the optical color curves $B-V, V-R$ and $V-I$, for SN 1997br in Figs. 7-9. We also show data from several other SNe Ia (1991T, 1989B, 1994D, and 1991bg) for comparison. We correct the SN 1997br data for a color excess of $E(B-V)$=0.35 mag (which we derive below), and follow Wells et al. (1994) in correcting the data for SN 1989B with $E(B-V)$=0.37 mag. A reddening of $E(B-V)$=0.04 is assumed for SN 1994D (Richmond et al. 1995). There is no reddening for SN 1991bg (Filippenko et al. 1992b). To calculate the extinction in the B, V, R, and I passbands we adopt the average interstellar extinction curve given in Table 2 of the review by Savage & Mathis (1979). In the discussion below, we denote any dereddened quantity with a superscript zero, such as $(B-V)^0$; values which lack the superscript are not corrected for reddening.

The $B-V$ color of SN 1997br shows a well-defined curve that conforms fairly well to those of SNe 1991T, 1989B, and 1994D, but differs significantly from that of the peculiar, subluminous SN 1991bg. At the time of the discovery (-9 days), SN 1997br has an observed color $B-V$=0.31 mag,corresponding to an intrinsic color $(B-V)^0$ = -0.04 mag for $E(B-V)$=0.35 mag. It then becomes progressively bluer, reaching a minimum value of $(B-V)^0 = -0.14$ mag at 4 days before the B maximum, and reddens again after this. At the time of B maximum the color is estimated to be $(B-V)^0$=-0.03. After B maximum the $B-V$ color of SN 1997br becomes progressively redder than that of SN 1991T ($\Delta(B-V) \approx$0.12 mag at 25 days), because SN 1997br has a more rapid decline rate in the B-band after its maximum. Both SN 1991T and SN 1997br reach about the same $B-V$ color, $(B-V)^0 \approx 1.1$, about 30 days after maximum. SN 1994D and 1989B seem to reach their peaks earlier (25 days after B maximum). Subsequently, the $B-V$ colors for

all SNe Ia (including SN 1991bg) turn slowly to the blue again.

The $V - R$ color of SN 1997br in Fig. 8 shows a similar pattern of evolution as those of SNe 1989B, 1991T and 1994D, but seems slightly bluer before 35 days after maximum. The agreement between the $V - R$ color of SN 1997br and that of SN 1991T is quite good, except during the time from -10 days before and 10 days after B maximum, in which time SN 1991T had very sparse observations.

The $V - I$ colors of these five SNe Ia (Fig. 9) show more variations than do the $B - V$ and $V - R$ colors. It is thus striking that the curve of SN 1997br is so similar to that of SN 1991T. Different SNe seem to reach their reddest $V - I$ colors at different epochs: SN 1991bg does it at day 17, SN 1994D at day 25, SN 1989B at day 35, and SNe 1997br and 1991T at day 40.

In general, all $B - V$,$V - R$, and $V - I$ color curves have similar a blue–red–blue pattern of evolution. Each color curve have a minimum and a maximum, but the times of these minima and maxima differ significantly. The $B - V$ color reaches its bluest value at about day -4 and its reddest value at about day 25-30; the $V - R$ and $V - I$ colors do this at day 10 and day 20-40, respectively.

2.4. Extinction

Conspicuous interstellar Na I D absorption lines are present in our low-resolution spectra of SN 1997br (Sec. 3), implying substantial reddening by intervening material in the Milky Way and in the host galaxy ESO576-G40. In this section we will attempt to derive the amount of interstellar extinction towards SN 1997br in two ways: by comparing its optical colors with those of other type Ia SNe, and by measuring the strength of interstellar absorption features in its spectra.

Considering the similar photometric behavior of SN 1997br and SN 1991T, we might assume that they should have similar color evolution and intrinsic colors at maximum light. We can then measure the relative amount of extinction between them very easily. Comparing the colors at the time of maximum in the B-band, we find differences of

$(B - V)_{97br}$ - $(B - V)_{91T} = 0.19$,

$(V - R)_{97br}$ - $(V - R)_{91T} = 0.14$, and

$(V - I)_{97br}$ - $(V - I)_{91T} = 0.35$ mag.

With our adopted extinction coefficients these values imply that $\Delta E(B - V)$ equals 0.19, 0.21, 0.22 mag, respectively, between SN 1997br and 1991T.

The reddening of SN 1991T, however, is uncertain. Filippenko et al. (1992a) and Ruiz-Lapuente et al. (1992) estimated $E(B - V)$ values of 0.13 and 0.34 mag, respectively,

based on interstellar Na I D lines in the parent galaxy. Phillips et al. (1993) estimated a reddening of $E(B-V)$=0.13 for SN 1991T based on the assumption that type Ia SNe share the same intrinsic $(B-V)$ color of 0.0 mag at B maximum. Jeffery et al. (1992), on the other hand, ruled out a reddening larger than 0.2 mag based on comparisons of spectra of SN 1991T and 1990N. Adopting $E(B-V) = 0.13$ mag for SN 1991T, we get $E(B-V)$ values of 0.32, 0.34, and 0.35 mag for SN 1997br from our color excesses in $B-V$, $V-R$, and $V-I$ respectively.

In our low-resolution spectra for SN 1997br we measured the total equivalent width (EW) of the Na I D lines (including the Galactic component) to be EW = 1.85 ± 0.1 Å. Adopting the prescription discussed by Filippenko et al. (1990) for SN 1987M, we derive a reddening of $E(B-V)$= 0.39 mag for SN 1997br. This estimate, however, is quite uncertain. For Galactic stars, the uncertainty in the relationship between the Na I D EW and $E(B-V)$ is large (e.g., Hobbs 1978). Although the conversion factor adopted by Filippenko et al. (1990) generally appears to underestimate the extinction, Jeffery et al. (1991) pointed out that this approach might actually overestimate the extinction. In any case, we consider the EW of the interstellar Na I D lines to be only an approximate indicator of the reddening.

In this paper we adopt a reddening of $E(B-V) = 0.35 \pm 0.10$ for SN 1997br.

3. Spectroscopy

3.1. Observations and Reductions

The spectroscopic observations were done mostly with the BAO 2.16-m telescope using the Photometrics spectrograph equipped with a Tektronix 1024 x 1024 pixel CCD. We also report here the spectra of SN 1997br obtained with the Lick 3-m Shane telescope (+ Kast CCD spectrograph; Miller & Stone 1993). The journal of observations is given in Table 4.

All of the optical spectra were reduced and calibrated using standard techniques. Wavelength calibrations were carried out via comparison Fe-Ar or He lamp exposures taken at the position of the supernova. The spectra were corrected for continuum atmospheric extinction using mean extinction curves for BAO and Lick; also, telluric lines were removed from the Lick (but not BAO) data. The final flux calibrations were derived from observations of one or more spectrophotometric standard stars (Oke & Gunn 1983). The spectra were obtained at large airmasses because of the object's southern declination (-22^o). For spectra obtained at Lick, particular care was taken to always align the slit along the parallactic angle, to avoid chromatic effects in the data (Filippenko 1982). This procedure was not adopted at BAO, however, and it may cause some problems for the continuum shape of the spectra. Comparison of data obtained at BAO and Lick at similar epochs (e.g., the two spectra at day -4 in Fig. 10), however, reveals significant differences only at the

extreme blue end, so this problem is not serious.

Our final set of spectra covering the period from 9 days before to 81 days after B maximum is displayed in Fig. 10. The first spectrum we obtained at BAO 9 days before maximum (Apr 11 UT) clearly illustrate the pecularities initially reported for SN 1991T – the blue and nearly featureless continuum, and the two major absorption lines at approximately 4270 and 4975 Å. The biggest anomaly, however, is the absence of Si II λ6355 and the Ca II H & K lines. The latter features are barely visible in the spectrum obtained on Apr 16 UT (4 days before B maximum).

As with the photometry, there is a big gap from 4 days before to 8 days after B maximum because of poor weather and the object's proximity to the bright moon. During this period dramatic changes occur, so the spectrum at day +8 is quite different from that at day -4. The continuum becomes considerably redder, and conspicuous lines of Si II λ6355, Ca II (H, K and IR triplet), and other intermediate-mass elements (S, Mg, etc.) appear in the day +8 spectrum. The spectrum now clearly resembles that of a Type Ia supernova, although the strengths of all intermediate-mass element absorption lines are relatively weaker than in normal SNe Ia. These data leave no doubt that SN 1997br is a genuine (though peculiar) type Ia event like SN 1991T.

Of particular interest is the evolution of Si II λ6355, which is the defining feature of type Ia SNe. Spectra taken earlier than 4 days before B maximum don't show significant evidence of this line (Fig. 10). A weak Si II λ6355 line appears in the day -4 spectrum, showing a broad absorption (FWHM 9000 km/s) centered at 6150 Å and with the blue edge corresponding to a velocity of 18000 km/s. Although this value is smaller than that measured in SN 1990N on day -14 (25000 km/s; Leibundgut et al. 1991) and in SN 1994D on day -11 (21600 km/s; Patat et al. 1996), it still indicates that the Si synthesized during the explosion extends well beyond the limit fixed by the unmixed W7 deflagration model (15000 km/s; Nomoto et al. 1984), as pointed out by several other authors (Mazzali et al. 1993; Kirshner et al. 1993).

In the second spectrum (day +8), the Si II λ6355 absorption line appears well developed, but considerably narrower (FWHM 6500 km/s), with a blue edge corresponding to a velocity of 15500 km/s. The absorption component moves slightly to the red in the spectra of days +10 and +12. Meanwhile, other features appear and contaminate the Si II line, most notably its red side (probably Fe II $\lambda\lambda$6456, 6518 at $\sim$ 6270 Å). Blueward of the line, there may be some Fe II $\lambda\lambda$6238, 6248 at $\sim$ 6050 Å. These changes can be seen most dramatically in the day +21 and +24 spectra, where the Si II λ6355 line is heavily obscured by these Fe II lines, and it disappears thereafter.

This behavior of the Si II λ6355 line doesn't follow that defined by the template spectral evolution of typical SNe Ia like SN 1989B (Wells et al. 1994) and SN 1994D (Patat et al. 1995; Filippenko 1997), which show a strong Si II λ6355 line at times well before and near B maximum. The later appearance, the earlier disappearance, and the general

weakness of the Si II λ6355 line in SN 1997br suggest that the Si layers in the ejecta of the SN may be confined to a very narrow velocity region, and the abundance of Si in the ejecta may be less than normal, as we will further discuss below.

To do a thorough comparison between the spectroscopic behavior of SN 1997br, SN 1991T, and typical SNe Ia like SN 1994D, we plot the spectra of these 3 SNe at different epochs (days -9, -3,+10,+14,+21,+51) in Figs. 11 to 16. All the spectra have been dereddened ($E(B-V) = 0.35$ mag for SN 1997br; $E(B-V) = 0.13$ mag for SN 1991T; $E(B-V) = 0.04$ mag for SN 1994D as derived by Richmond et al. 1995) and have been corrected for the observed galaxy redshifts. The line identifications adopted here are taken from Kirshner et al. (1993), Jeffery et al. (1992), and Mazzali et al. (1995).

At times before and around maximum light the SN Ia spectrum is produced by the outermost material in the ejecta and is composed mainly of lines of intermediate-mass elements for normal cases (Branch et al. 1985; Kirshner et al. 1993). This can be seen clearly in the day -9 spectrum of SN 1994D in Fig. 11; it is dominated by lines of Si II, S II, Mg II, Ca II, and O I. The spectra of SN 1997br and SN 1991T are similar to each other but significantly different from that of SN 1994D. The two main absorption features are believed to be multiplets of Fe III λ4404 and Fe III λ5129, respectively (Jeffery et al. 1992; Ruiz-Lapuente et al. 1992). This peculiar phenomenon of Fe-dominated type Ia pre-maximum spectra is explained by many authours in terms of abnormal abundances and/or abnormal temperatures in the ejecta of the SN (Filippenko et al. 1992a; Ruiz-Lapuente et al. 1992; Phillips et al. 1992; Jeffery et al. 1992).

By day -3, the spectrum of SN 1994D has changed significantly. Si II λ3858 is well separated from the Ca II H & K lines, and is stronger, as is the Si II λ4560 line. Si II λ6355 now has a well-developed P-Cygni profile. S II λ5468 and S II $\lambda\lambda$5612, 5654 form the characteristic "W"-shaped feature in the 5200 – 5600 Å region. The Ca II H & K lines, however, are less prominent than in the day -9 spectrum. The spectra of SN 1997br and SN 1991T are still dramatically different from that of SN 1994D. In the day -4 spectrum of SN 1997br, the characteristic feature of SNe Ia, Si II λ6355, appears only marginally at 6100 Å, accompanied by other Si lines at 4400 Å (Si III λ4560), 4800 Å (Si II λ5051), and probably 3700 Å (Si II λ3858). There is also a hint of the Ca II H & K lines at 3800 Å. S II (the "W" shape) may be responsible for the weak flat-bottomed absorption in the 5200 – 5400 Å region. Our day -3 spectrum of SN 1991T doesn't extend out to the Si II λ6355 line, but Phillips et al. (1992) report that Si II λ6355 line was weakly present at this epoch, and in most respects the spectrum is quite similar to that of SN 1997br.

The spectra of these 3 SNe about 10 days after B maximum (Fig. 13) differ from the premaximum ones. As marked in Fig. 13, Fe II and Co II lines begin to appear in the spectrum of SN 1994D, and Na I D contributes to the absorption at 5750 Å. O I λ7773 and the Ca II IR triplet become much stronger, while the "W"-shaped S II lines become much weaker than in the day -3 spectrum. More significant changes happen to the spectra

of SN 1997br and SN 1991T: the appearance of their spectra is now generally similar to that of SN 1994D. Intermediate-mass element lines of Si, O, Ca, and S appear in their spectra, although their intensities are relatively weaker than in SN 1994D. Fe-peak element lines, on the other hand, are better developed in the spectra of SN 1997br and SN 1991T. Comparison of the spectra of SN 1997br and SN 1991T at this epoch reveals minor yet interesting differences – the Si II and the "W" shaped S II lines are slightly stronger in SN 1991T, while the Fe II and Co II lines are better developed in SN 1997br. The red wing of the Si II λ6355 line of SN 1997br, even at this phase, shows contamination by Fe II $\lambda\lambda$6456, 6518. This might indicate that spectra of SN 1997br have a shorter duration of intermediate-mass element lines and a faster transition to the Fe-peak element lines after B maximum than do those of SN 1991T.

More evidence for this can be found in the day +14 spectra in Fig. 14, where the Si II λ6355 line of SN 1997br shows a flat-bottomed absorption due to the increased strength of Fe II, while those of SN 1991T and SN 1994D still retain a well-defined P-Cygni profile. As marked in Fig. 14, the spectrum of SN 1997br also shows stronger evidence of Fe II $\lambda\lambda$6238, 6248 and Co II λ4152 absorption. The three spectra exhibit quite different features around the 5200 – 5600 Å region. SN 1994D shows a notch of absorption at 5340 Å that might be caused by Fe II λ5535; SN 1997br also shows this absorption and possibly its emission component at around 5500 Å. SN 1991T, however, doesn't show this absorption, and may still have a hint of the "W"-shaped S II lines.

Inspection of the day +21 spectra of the three SNe (Fig. 15) reveals that this trend continues. Fe II and Co II lines now dominate all three spectra. SN 1994D still shows a distinct Si II λ6355 line, while SN 1991T may have a hint of its existence in the flat-bottomed absorption at around 6100 Å. SN 1997br, on the other hand, is dominated by Fe II $\lambda\lambda$6456, 6518 lines. In the 5200–5600 Å region, both SN 1994D and SN 1997br exhibit absorption at 5300 Å and prominent emission at 5500 Å, while SN 1991T only has the absorption. All three spectra show quite similar features in the region blueward of 5400 Å, although it can be seen that the emission lines at 4600 Å (Fe II λ4555) and 5000 Å (Fe II λ5018) have comparable strengths in SN 1994D, while the 4600 Å emission is stronger than that at 5000 Å in SN 1997br and in SN 1991T.

Given all the differences we have seen in the spectral evolution of these three SNe so far, the overall similarity of their nebular phase spectra (about 50 days after B maximum in Fig. 16) is quite impressive. The difference in the 5200 – 5600 Å region disappears: all of them show strong emission at 5500 Å. The intensity ratios of the emission lines at 4600 Å (Fe II λ4555) to that at 5000 Å (Fe II λ5018) are similar. Careful inspection of the spectra reveals, however, some minor difference among them. Even at this late phase, SN 1994D still shows a weak Si II λ6355 line at 6100 Å. The Na I D line is also stronger in SN 1994D than it is in SN 1997br and SN 1991T. More evidence of differences between the spectra can be seen at around 4800 Å, 5400 Å, 6000 Å, and 7000 Å.

Our comparison shows clearly that the peculiarity of the spectroscopic behavior of SN 1997br and SN 1991T is not confined only to before and around maximum as reported by Phillips et al. (1992), but extends to the nebular phase. At any given epoch, SN 1994D (normal SN Ia) always shows stronger intermediate-mass element lines, while SN 1997br and SN 1991T show stronger and better developed Fe-peak element lines.

Moreover, although the overall spectroscopic behavior of SN 1997br is similar to that of SN 1991T, there are still important differences. Specifically, SN 1997br has a faster transition to Fe-peak element lines in the nebular phase. If we explain the peculiar spectroscopic behavior of these two SNe in terms of their abundance anomaly, this might mean that SN 1997br has shallower and thinner layers of intermediate-mass elements in the ejecta than does SN 1991T.

An abundance anomaly, however, might not be the only way to account for the peculiarities and differences seen in the spectra of SN 1997br and SN 1991T: different temperature evolution of the photosphere may play some role. As can be seen in the pre-maximum spectra (Figs. 11 and 12), SN 1997br and SN 1991T are somewhat bluer than SN 1994D and thus may have higher photosphere temperatures. This higher temperature favors the production of Fe III lines but not of intermediate-mass element lines (Mazzali et al. 1995). As the SNe evolve, their photospheric temperatures drop, and intermediate-mass element lines begin to form. Evidence that SN 1997br had a faster drop in temperature than SN 1991T can be found in Fig. 13, 14, and 15, where the continuum of SN 1997br is redder than that of SN 1991T and is similar to that of SN 1994D. The slower temperature evolution of SN 1991T may also be responsible for its different evolution in 5200–5600 Å region on days +14 and +20. The bluer continuum of SN 1991T compared with that of SN 1997br on days +14 and +20 is also consistent with the photometric behavior of these two SNe seen in Fig. 7: SN 1991T is bluer at epoch 10 to 30 days after B maximum in the $(B-V)$ color.

The expansion velocities as inferred from observed minima in the spectra may provide some clue to the nature of SN Ia explosions (Branch et al. 1988). Fig. 17 shows the derived expansion velocities of the Fe III λ4404, Fe III λ5129, Fe II λ4555, and Si II λ6355 lines for SN 1997br and SN 1991T, together with those derived from Si II λ6355 for SN 1981B (Branch et al. 1983), SN 1986G (Phillips et al. 1987), SN 1989B (Wells et al. 1994), SN 1991bg (Leibundgut et al. 1993), and SN 1994D (Patat et al. 1996). Comparison of data reveals that the expansion velocities of the Fe lines (Fe III λ4404, Fe III λ5129, Fe II λ4555) are slightly higher in SN 1991T than in SN 1997br, while the velocities of Si II λ6355 are higher in SN 1997br than in SN 1991T. This indicates that SN 1997br indeed has a relatively shallower (and thus higher velocity) layer of Si compared to SN 1991T, consistent with our earlier discussion. The Si II velocities for SN 1997br are remarkable in their slow decline (-11500 km/s to -10500 km/s) over the 22 day period (-4 to +18 days) during which this line was measurable. SN 1991T shows similar behavior, as reported by Phillips et al. (1992), and this might imply that the Si zone in the expanding ejecta of SN 1997br was

confined to a fairly restricted layer characterized by velocities in the range 10500–11500 km/s (for SN 1991T the velocity range is 9000–10000 km/s).

The Fe III λ4404 and Fe III λ5129 line velocities show an abrupt change in the decline rate around day -7. A similar phenomenon has been found in SN 1990N (Leibundgut et al. 1991) and in SN 1994D (Patat et al. 1995) for the Si II λ6355 line, and was explained in terms of changes in the density gradient and increased amounts of absorbing layers as the photosphere recedes.

4. Discussion

4.1. Absolute magnitude of SN 1997br

Having measured the peak magnitude of each light curve, and found a value for the extinction, we lack only one piece of information needed to calculate the absolute magnitude of SN 1997br: the distance to ESO576-G40.

This galaxy, also named MCG-04-32-007 and PGC 46574, is listed as a member of one group of galaxies, namely group 345 of the Lyon Group of Galaxies (LGG) Catalog (Garcia 1993). Other members and their heliocentric recession velocities are NGC 5084 (1514 km/s), NGC 5087 (1625 km/s), NGC 5134 (1550 km/s), and ESO 576-G50 (1781 km/s). The heliocentric velocity of ESO576-G40 measured by several groups using different methods (e.g., Fairall et al. 1992; Han 1992; Mathewson et al. 1992; Fouque et al. 1990) yields values between 2055 and 2086 km/s. The luminosity-weighted mean recession velocity of the group is calculated to be 1583 km/s (Garcia 1993).

Zeilinger, Galleta, & Madsen (1990) found that ESO576-G40 appeared to be perturbed by the presence of NGC5084 in their optical image. Carignan et al. (1997) further suggested that NGC 5084, as one of the most massive disk galaxies known, had survived the accretion of several satellite galaxies similar to ESO576-G40. All these studies suggest that ESO576-G40 may have a physical relationship with NGC 5084 and thus be at the same distance. In this sense we can use the recession velocity for the group, 1583 km/s, as a distance measurement for ESO576-G40.

Mathewson et al. (1992) presented photometric and spectroscopic observations of 1355 southern spiral galaxies and determined their distances and peculiar velocities via the Tully-Fisher (TF) relation. All their distances are measured relative to the Fornax cluster whose distance was taken to be 1340 km/s. They measured recession velocities of 2085 km/s (heliocentric) and 2403 km/s (CMB frame) for ESO576-G40. The TF distance to ESO576-G40 was measured to be 1248 km/s after the Malmquist bias correction. This distance, with a peculiar velocity of 1155 km/s relative to the CMB frame, may have large associated uncertainties because ESO576-G40 is a highly inclined (nearly edge-on) galaxy

and is not well measured with the TF relation, so we are reluctant to use this distance measurement for ESO576-G40.

Adopting a distance of 1583 km/s for ESO576-G40 and a Hubble constant of 65 km s^{-1} Mpc^{-1} (Hamuy et al. 1996), the extinction-corrected absolute magnitudes for SN 1997br are listed below,

M_B = -19.29±0.42,

M_V = -19.28±0.32,

M_R = -19.02±0.25,

M_I = -18.97±0.18.

The errors of the magnitudes are the sums in quadrature of the uncertainties in peak magnitudes and the uncertainties in extinctions.

From the absolution magnitudes we can see that SN 1997br may be somewhat more luminous than typical SNe Ia. This is consistent with the fact that SN 1997br shares many similarities with the overluminous SN 1991T. The absence of a better distance measurement for its host galaxy, however, prevents us from making definitive conclusions regarding the absolute magnitudes of SN 1997br.

4.2. Heterogeneity of type Ia SNe

It is well known that SNe Ia display a remarkable degree of similarity, more than any other subclass of SNe, and their spectral evolution and light curves follow a reproducible pattern (Minkowski 1939; Kirshner et al. 1973; Wells et al. 1994). During the past 15 years, however, spectroscopic and photometric peculiarities have been reported with increasing frequency in well-observed SNe Ia, and it is now settled that SNe Ia are not perfectly homogeneous (see Filippenko 1997 for a review).

Nevertheless, Branch et al. (1993) conclude that the observational sample of SNe Ia is strongly peaked at spectroscopically normal (89% in a sample of 84 SNe Ia studied). We emphasize here, however, that this rate may be overestimated since most of the spectra of these SNe Ia were taken at or after their optical maxima, while the peculiarity of some SNe Ia is most conspicuous before their optical maxima (e.g., SN 1991T and SN 1997br). They also did not account for the observational bias against subluminous SNe Ia like SN 1991bg.

A striking statistic from the BAO SN survey is that, among the 12 SNe Ia discovered in 1.5 years, 4 (33%) are peculiar. SN 1997br (Li et al 1997a), SN 1997cw (Qiao et al. 1997b), and SN 1998ab (Wei 1998) are SN 1991T-like, while SN 1997cn (Li et al. 1997b) is SN 1991bg-like. Nearly all SNe Ia discovered by the BAO SN survey were found before their optical maximum. Though the SN Ia sample from the BAO SN survey is small and our

derived rate (33%) is subject to small-number statistics, it does suggest that the frequency of peculiar SNe Ia might be larger than that reported by Branch et al. (1993), and it stresses the importance of discovering and observing these SNe before their optical maxima.

4.3. Models of SNe Ia

It is generally accepted that SNe Ia are thermonuclear explosions of carbon-oxygen white dwarfs with mass very near the Chandrasekhar mass (M_{ch}) of 1.4 $M_{\odot}$. From the theoretical standpoint the key question is how the burning front or flame propagates through the white dwarf. Models of SNe Ia proposed in the past three decades can be divided into three classes: deflagration (turbulent convective subsonic propagation; e.g., Nomoto et al. 1976), detonation (a supersonic shock wave that initiates burning; e.g., Arnett 1969), and delayed detonation (the flame starts as a deflagration and accelerates into a detonation later; e.g., Khokhlov 1991).

Recently a large variety of models of these three classes have been investigated by several papers of Höflich, Khokhlov, and Muller (see references in Höflich et al. 1995). They conclude that no single model is capable of representing the whole range of SNe Ia. In general, pure detonation models burn the entire star into iron-peak elements and can be ruled out for SNe Ia because of the presence of significant intermediate-mass elements. Diffferent variations of the delayed detonation models, on the other hand, can be used to explain various SN Ia light curves (but not necessarily the explosions themselves). They are also used to explain the peculiar behavior of Fe-dominated pre-maximum spectra of SN 1991T (Filippenko et al. 1992a; Ruiz-Lapuente et al. 1992). Deflagration models may be necessary to explain subluminous SNe Ia like SN 1991bg (Filippenko et al. 1992b; Leibundgut et al. 1993).

Despite the successes of these models, the physics of the explosion is far from being completely solved. All of them need to be parameterized to avoid intractable three-dimensional calculations, and none has a rise time long enough to be consistent with the observations (e.g., > 17.5 days for SN 1990N; Leibundgut et al. 1991). The initial explosive state of the white dwarf and the history leading to this state are not well understood (see reviews by, e.g., Woosley & Weaver 1986; Wheeler & Harkness 1990; Branch et al. 1995).

The physical conditions of different white dwarfs at the time of explosion may be dissimilar, and this could cause the heterogeneity seen in SNe Ia. Possible differences in the physics of the white dwarfs are as follows,

1) *Composition*. A helium white dwarf will have a different explosion than a carbon-oxygen white dwarf.

2) *Temperature*. Variations in temperature may be caused by different accretion rates

and different compositions of the accreted matter from the companion star.

3) *Magnetic field.* No models that account for the magnetic fields of white dwarfs are available, yet they might affect the explosion considerably.

4) *Rotation.* No models that account for the rotation of white dwarfs are available either, yet rotation is known to change the explosion characteristics of Type II SNe considerably (e.g., Mönchmeyer 1990).

5) *Mass.* Because of differences in composition, temperature, magnetic field, rotation, and other factors of the white dwarf, the Chandrasekhar mass is not a unique number, and explosions may occur at different masses. At least one SN Ia, SN 1991bg, may have exploded at a much smaller mass than 1.4 $M_{\odot}$ (Filippenko et al. 1992b; Leibundgut et al. 1993).

The outcome of a *decelerated detonation* (i.e., a detonation initializes the explosion of a white dwarf, then decelerates and turns into a deflagration) has not been carefully studied by theorists, yet it might be a promising model for some SNe Ia (normal or SN 1991T-like). When the detonation propagates outward, it may decelerate because of decreasing matter density (less burning material density), decreasing temperature (more energy needs to be absorbed to ignite burning), and whatever other reasons. We propose this model for the following reasons:

(1) It may provide a model for normal SNe Ia. The outer part of the ejecta will consist of a deflagration composition that has been favored by spectral simulations. Moreover, the expansion velocity will be higher than that of pure deflagration models like W7 because of the detonation origin. This is consistent with observations of several recent SNe Ia, which require higher outermost expansion velocities than model W7 (e.g., Leibundgut et al. 1991; Patat et al. 1996; Kirshner et al. 1993).

(2) It may also account for SN 1991T-like SNe Ia. When the initial detonation is energetic enough, it will propagate as a detonation until reaching the outermost part of the envelope, where it can become a deflagration. Events like this may have a higher luminosity, higher photospheric temperature, and less mass consisting of intermediate-mass elements in the outermost envelope, and may result in events like SN 1991T and SN 1997br.

The deceleration in our proposed model is in direct contrast to the acceleration inherent in the very successful delayed detonation model, which has been widely accepted and used. However, there isn't rigorous physical support for the mechanism of acceleration or deceleration, so the outcomes of both scenarios should be investigated; the decelerated detonation model may yield some fruitful results.

5. Conclusions

In this paper we reported our photometric and spectroscopic observations of the peculiar type Ia SN 1997br in ESO576-G40. The overall photometric and spectroscopic behavior of SN 1997br closely resembles that of the peculiar type Ia SN 1991T, but with some noticeable differences.

The $BVRI$ light curves of SN 1997br are very similar to those of SN 1991T, with a slightly faster initial decline rate after B maximum in the B band. The optical color curves also resemble those of SN 1991T. The well-sampled data before the optical maximum show clearly that SN 1997br rises more slowly and has a wider peak than do normal SNe Ia like SN 1994D.

An extinction estimate of $E(B-V) = 0.35\pm0.10$ mag is obtained for SN 1997br by comparing the mutlicolor light curves of SN 1997br to those of SN 1991T, and by applying an empirical relationship between extinction and the equivalent width of interstellar Na I D lines. Lacking an accurate distance estimate for its host galaxy, however, we cannot obtain conclusive results for its unextinguished luminosities.

We have compared the spectroscopic evolution of SN 1997br to that of SN 1991T and the normal type Ia SN 1994D at various epochs. The spectroscopic evolution of SN 1997br is similar to that of SN 1991T, and is peculiar relative to SN 1994D. Before B maximum the spectra show two dominant Fe III features centered at 4270 and 4970 Å superimposed on an otherwise nearly featureless blue continuum. As the SN ages it shows gradually the characteristic type Ia features – Si II λ6355 and lines of other intermediate-mass elements. SN 1997br seems to exhibit an earlier transition to the Fe-peak element line dominant phase than both SN 1994D and SN 1991T. The Si λ6355 line of SN 1997br shows a shorter duration than does that of SN 1991T. Our comparison demonstrates that the spectroscopic peculiarity of SN 1997br (and SN 1991T) exists not only before and at optical maximum, but also in the nebular phase at a reduced level.

SN 1997br and other objects demonstrate the heterogeneity of SNe Ia, which we believe is produced by differences in the physical conditions of the white dwarf progenitors and in the explosion mechanisms. In particular, we propose a "decelerated detonation" model which might be promising in several ways.

We would like to thank all observational astronomers at the 2.16m telescope of BAO, in particular J.Y. Wei, X.J. Jiang, D.W. Xiu, L. Cao, J.Z. Li, X.Y. Dong and W. Liu, for their help in our observations of SN 1997br. W.D. Li has benefited greatly from discussions with Prof Z.W. Li of Beijing Normal University and Dr. Adam Riess of the University of California at Berkeley. We also thank Ricardo Covarrubias of CTIO for providing us with

the calibration observations of the SN 1997br field. This work is supported by NSF grant AST-9417213 to A.V.F. and by the National Science Foundation of China. We are grateful to Sun Microsystems Inc. (Academic Equipment Grant Program), Photometrics Ltd., the National Science Foundation, and the Sylvia and James Katzman Foundation for donations that made KAIT possible.

REFERENCES

Arnett, W.D., 1969, Ap&SS, 5, 180

Branch, D., et al., 1983, ApJ, 270, 123

Branch, D., Doggett, J.B., Nomoto, K., & Thielemann, F.-K., 1985, ApJ, 294, 619

Branch, D., Drucker, W., & Jeffery, D.J., 1988, ApJ, 330, L117

Branch, D., Fisher, A., & Nugent, P., 1993, AJ, 106, 2383

Carignan, C., Cote, S., Freeman, K.C., & Quinn, P.J., 1997, AJ, 113,1585

Cousins, A.W.J., 1981, S. Afr. Astron. Obs. Circ., 6, 4

Fairall, A.P., et al., 1992, AJ, 103, 11

Ford, C.H., et al., 1993, AJ, 106, 1101

Filippenko, A.V., 1982, PASP, 94, 715

Filippenko, A.V., 1989, PASP, 101, 588

Filippenko, A.V., 1997, ARAA, 35, 309

Filippenko, A.V., Porter, A.C., & Sargent, W.L.W., 1990, AJ, 100, 1575

Filippenko, A.V., et al., 1992a, ApJ, 384, L15

Filippenko, A.V., et al., 1992b, AJ, 104, 1543

Fouque, P., et al., 1990, A&AS, 86, 473

Garcia, A.M., 1993, A&AS, 100, 47

Hamuy, M., et al., 1994, AJ, 108, 2226

Hamuy, M., et al., 1996a, AJ, 112, 2438

Hamuy, M., et al., 1996b, AJ, 112, 2391

Han, M., 1992, ApJS, 81, 35

Hobbs, L.M.,1978, ApJS, 38, 129

Höflich, P., 1995, ApJ, 443, 89

Jeffery, D.J., et al., 1992, ApJ, 397, 304

Jeffery, D.J., Branch, D., Filippenko, A.V., & Nomoto, K., 1991, ApJ, 377, L89

Johnson, H.L., Mitchell, R.I., Iriarte, B., & Wisniewski, W.Z., 1966, Commun. Lunar Plant. Lab, 4, 99

Khokhlov, A., 1991, A&A, 245, 114

Kirshner, R.P., Oke, J.B., Penston, M.V., & Searle, L., 1973, ApJ, 185, 303

Kirshner, R.P., et al., 1993, ApJ, 415, 589

Landolt, A.U., 1992, AJ, 104, 340

Leibundgut, B., et al., 1991, ApJ, 371, L23

Leibundgut, B., et al., 1993, AJ, 105, 301

Li, W.D., Qiu, Y.L., Qiao, Q.Y., Hu, J.Y. (the BAO SN survey), 1997a, IAU Circ. No. 6623

Li, W.D., 1997, IAU Circ. No. 6642

Li, W.D., et al., 1997b, IAU Circ. No. 6661

Mathewson, D.S., Ford, V.L., & Buchhorn, M., 1992, ApJS, 81, 413

Maza, J., et al., 1994, ApJ, 424, L107

Mazzali, et al., 1993, A&A, 269, 423

Mazzali, P.A., Danziger, I.J., & Turatto, M., 1995, A&A, 297, 509

Miller, J.S., & Stone, R.P.S., 1993, Lick Obs. Tech. Rep., No. 66

Minkowski, R., 1939, ApJ, 89, 156

Mönchmeyer, R., 1990, Ph.D. thesis, Tech. Univ. Munchen

Nomoto, K., Sugimoto, D., & Neo, S., 1976, Ap&SS, 39, 137

Nomoto, K., Thielemann, F.K., & Yokoi, K., 1984, ApJ, 286, 644

Oke, J.B., & Gunn, J.E., 1983, ApJ, 266, 713

Patat, F., et al., 1996, MNRAS, 278,111

Phillips, M.M., et al., 1987, PASP, 99, 592

Phillips, M.M., 1993, ApJ, 413, L105

Phillips, M.M., et al., 1992, AJ, 103, 1632

Qiao, Q.Y., Wu, H., Wei, J.Y., Li, W.D., 1997a, IAU Circ. No. 6623

Qiao, Q.Y.,Qiu, Y.L., Li, W.D.,Hu, J.Y., 1997b, IAU Circ. No. 6699

Richmond, M.W., et al., 1995, AJ, 109, 2121

Ruiz-Lapuente, P., et al., 1992, ApJ, 387, L33

Savage, B.D., & Mathis, J.S., 1979, ARA&A, 17, 73

Schmidt, B.P., et al., 1993, AJ, 105, 2236

Wei, J.Y., & Li, W.D., (the BAO SN survey), 1998, IAU Circ. No. 6858

Wells, L.A., et al., 1994, AJ, 108, 2233

Wheeler, J.C., & Harkness, R.P., 1990, Rep. Prog. Phys., 53, 1467

Woosley, S.E., & Weaver, T.A., 1986, ARA&A, 24, 205

Zeilinger, W.W., Galletta, G., & Madsen, C., 1990, MNRAS, 246, 324

This manuscript was prepared with the AAS LaTeX macros v4.0.

Fig. 1.— R-band KAIT image of the field of SN 1997br, with the 5 local standard stars marked. The size of the field is 5.38' × 5.38'. North is up and east is to the left.

Fig. 2.— The B, V, R, and I light curves of SN 1997br, along with the best χ^2-minimizing fits to the light curves of SN 1991T.

Fig. 3.— The B light curve of SN 1997br, together with those of SN 1991T (Hamuy et al. 1996b), SN 1989B (Wells et al. 1994), SN 1994D (Richmond et al. 1995), and SN 1991bg (Leibundgut et al. 1993). All light curves are shifted in time and magnitude to match that of SN 1997br (see text for more details).

Fig. 4.— Same as Fig. 3 but for the V light curve.

Fig. 5.— Same as Fig. 3 but for the R light curve. The R light curve of SN 1991T comes from Ford et al. (1993). The R and I light curves of SN 1991bg come from Filippenko et al. (1992b).

Fig. 6.— Same as Fig. 3 but for the I light curve.

Fig. 7.— The $B-V$ color curve of SN 1997br, together with those of SN 1991T (Phillips et al. 1992), SN 1989B (Wells et al. 1994), SN 1994D (Richmond et al. 1995), and SN 1991bg (Filippenko et al. 1992b; Leibundgut et al. 1993).

Fig. 8.— Same as Fig. 7 but for the $V-R$ color curve.

Fig. 9.— Same as Fig. 7 but for the $V-I$ color curve.

Fig. 10.— Spectra of SN 1997br; see Table 4 for details. The phases marked are relative to the date of B maximum. For presentation the spectra have been shifted by arbitrary amounts.

Fig. 11.— The day -9 spectrum of SN 1997br, together with the day -9 spectra of SN 1991T (Filippenko et al. 1992a) and SN 1994D (Patat et al. 1996). The spectra have been shifted by arbitrary amounts for clarity. Line identifications are taken from Kirshner et al. (1993), Jeffery et al. (1992), and Mazzali et al. (1995).

Fig. 12.— Same as Fig. 11 but for the day -4 spectrum of SN 1997br, the day -3 spectrum of SN 1991T, and the day -3 spectrum of SN 1994D.

Fig. 13.— Same as Fig. 11 but for the day +10 spectrum of SN 1997br, the day +11 spectrum of SN 1991T, and the day +10 spectrum of SN 1994D.

Fig. 14.— Same as Fig. 11 but for the day +14 spectra of SNe 1997br, 1991T, and 1994D.

Fig. 15.— Same as Fig. 11 but for the day +21 spectrum of SN 1997br, the day +20 spectrum of SN 1991T, and the day +21 spectrum of SN 1994D.

Fig. 16.— Same as Fig. 11 but for the day +51 spectrum of SN 1997br, the day +51 spectrum of SN 1991T, and the day +50 spectrum of SN 1994D.

Fig. 17.— Evolution of the expansion velocity as deduced from the minima of the Fe III λ4404, Fe III λ5129, Fe II λ4555, and Si II λ6355 absorptions for SN 1997br (open circles), SN 1991T (solid circles; measured from spectra in Filippenko et al. 1992a), SN 1981B (Branch et al. 1983), SN 1986G (Phillips et al. 1987), SN 1989B (Wells et al. 1994), SN 1991bg (Leibundgut et al. 1993), and SN 1994D (Patat et al. 1996).

Table 1. Magnitudes of local standard stars

Star	U	σ_U	B	σ_B	V	σ_V	R	σ_R	I	σ_I
A	14.646	0.017	14.344	0.004	13.524	0.002	13.029	0.004	12.527	0.005
B	18.198	0.204	17.219	0.025	15.961	0.008	15.302	0.013	14.669	0.016
C	16.873	0.085	16.497	0.017	15.645	0.007	15.155	0.011	14.684	0.014
D	17.250	0.090	16.446	0.017	15.509	0.007	14.973	0.011	14.479	0.013
E	–	–	20.307	0.281	18.336	0.046	17.200	0.067	15.779	0.071

arXiv:astro-ph/9903466v1 30 Mar 1999

Table 2. Photometric observations of SN 1997br. Phases are relative to the epoch of B maximum (JD=2450559.3)

Date DD/M/YY	J.D. - 2450000.0	Phase (days)	B	V	R	I	Telescope	Comments
11/4/97	550.5	−9	14.69	14.38	14.32	–	BAO	
12/4/97	551.5	−8	14.53	14.24	14.21	–	BAO	
13/4/97	552.5	−7	14.52	14.11	14.08	–	BAO	
14/4/97	553.5	−6	14.38	14.08	14.01	–	BAO	
15/4/97	554.5	−5	14.25	14.00	13.92	–	BAO	poor seeing
16/4/97	555.5	−4	14.18	13.96	13.90	–	BAO	
17/4/97	556.5	−3	–	13.91	13.87	–	BAO	
19/4/97	558.5	−1	–	13.86	13.78	–	BAO	
25/4/97	564.5	+5	14.23	13.80	13.74	–	BAO	bright moon
26/4/97	564.9	+6	14.26	13.77	13.85	13.70	KAIT	
28/4/97	567.4	+8	14.45	13.81	13.82	–	BAO	poor seeing
29/4/97	568.5	+9	14.46	13.82	13.86	–	BAO	
30/4/97	568.8	+10	14.57	13.83	13.94	13.78	KAIT	poor seeing
30/4/97	569.4	+10	–	13.92	13.90	–	BAO	clouds
02/5/97	570.8	+12	14.77	13.95	14.05	13.84	KAIT	
02/5/97	571.4	+12	–	13.97	14.05	–	BAO	
03/5/97	572.4	+13	15.01	13.99	14.00	–	BAO	
04/5/97	573.5	+14	15.02	14.07	14.05	–	BAO	
05/5/97	573.8	+15	15.07	14.15	14.14	13.87	KAIT	
06/5/97	574.9	+16	–	14.21	–	–	KAIT	clouds
07/5/97	575.8	+17	15.33	14.24	14.16	13.85	KAIT	
07/5/97	576.5	+17	–	14.28	14.09	–	BAO	
08/5/97	577.5	+18	–	14.32	14.14	–	BAO	clouds
10/5/97	578.8	+20	15.67	14.42	14.20	13.84	KAIT	
11/5/97	579.8	+21	15.74	14.47	14.22	13.84	KAIT	
13/5/97	581.8	+23	15.94	14.57	14.27	13.86	KAIT	
14/5/97	583.4	+24	–	14.60	14.30	–	BAO	clouds
16/5/97	585.4	+26	16.13	14.83	14.35	–	BAO	
17/5/97	585.8	+27	16.20	14.77	14.38	13.96	KAIT	
18/5/97	586.8	+28	16.24	14.81	14.40	13.96	KAIT	
24/5/97	593.4	+34	16.56	15.06	14.65	–	BAO	
25/5/97	593.8	+35	–	15.08	14.62	14.14	KAIT	poor seeing
28/5/97	596.8	+38	–	15.25	14.78	14.28	KAIT	
28/5/97	597.4	+38	16.66	15.20	14.81	–	BAO	
29/5/97	597.7	+38	–	15.28	14.84	14.32	KAIT	
29/5/97	598.4	+39	16.74	15.29	14.89	–	BAO	
31/5/97	599.8	+41	16.80	15.36	14.96	14.45	KAIT	
01/6/97	601.4	+42	–	15.40	15.05	–	BAO	
02/6/97	601.8	+43	16.89	15.51	15.08	14.58	KAIT	
03/6/97	603.4	+44	–	15.52	15.11	–	BAO	clouds
06/6/97	605.8	+47	–	15.62	15.26	14.77	KAIT	
08/6/97	607.7	+48	17.01	15.70	15.37	14.90	KAIT	
09/6/97	609.4	+50	16.96	15.73	15.45	–	BAO	
11/6/97	610.7	+51	17.00	15.78	15.48	15.06	KAIT	
11/6/97	611.4	+52	–	15.75	15.52	–	BAO	clouds
14/6/97	614.4	+55	–	15.80	15.59	–	BAO	
24/6/97	623.7	+64	–	16.05	15.94	15.60	KAIT	
25/6/97	625.4	+66	17.25	16.18	15.95	–	BAO	
26/6/97	626.4	+67	–	16.22	15.98	–	BAO	
28/6/97	626.7	+68	17.21	–	–	–	KAIT	

Table 3. Peak apparent magnitudes of SN 1997br

Filter	B	V	R	I
Epoch of Max.	Apr 20.3±1.5	Apr 23.4±1.0	Apr 23.2±1.0	Apr 19.8±2.0
Julian Date of Max. (- 2450000.0)	559.1±1.5	562.2±1.0	562.0±1.0	558.6±2.0
Magnitude at Max.	14.06±0.10	13.74±0.06	13.64±0.10	13.50±0.20

Table 4. Journal of Spectroscopic Observations

UT Date DD/M/YY	J.D. − 2450000.0	Phase (days)	range Å	equipment
11/4/97	550.2	−9	3800−8000	BAO−2.16
12/4/97	551.2	−8	4000−8000	BAO−2.16
13/4/97	552.2	−7	3800−8200	BAO−2.16
14/4/97	553.2	−6	4000−8400	BAO−2.16
16/4/97	554.8	−4	3200−10200	Lick−3.0
16/4/97	555.2	−4	3600−8200	BAO−2.16
28/4/97	567.1	+8	3400−9400	BAO−2.16
30/4/97	569.2	+10	3400−10600	BAO−2.16
02/5/97	571.1	+12	4000−8800	BAO−2.16
04/5/97	573.2	+14	3800−8800	BAO−2.16
08/5/97	577.1	+18	4000−10200	BAO−2.16
11/5/97	509.8	+21	3000−7000	Lick−3.0
14/5/97	583.1	+24	4000−8000	BAO−2.16
28/5/97	597.1	+38	3800−8400	BAO−2.16
06/6/97	605.8	+47	3400−10400	Lick−3.0
10/6/97	610.1	+51	3800−8400	BAO−2.16
26/6/97	626.1	+67	3800−8200	BAO−2.16
10/7/97	639.7	+81	4000−10000	Lick−3.0